American Mineralogist, Volume 101, pages 371–384, 2016

Crystal chemistry and light elements analysis of Ti-rich garnets

Emanuela Schingaro[1,*], Maria Lacalamita[1], Ernesto Mesto[1], Gennaro Ventruti[1], Giuseppe Pedrazzi[2], Luisa Ottolini[3], and Fernando Scordari[1]

[1]Dipartimento di Scienze della Terra e Geoambientali, Università degli Studi di Bari "Aldo Moro", via E. Orabona 4, I-70125, Bari, Italy
[2]Dipartimento di Neuroscienze, Università di Parma, via Volturno 39, I-43100, Parma, Italy
[3]CNR-Istituto di Geoscienze e Georisorse, Unità di Pavia, via A. Ferrata 1, I-27100 Pavia, Italy

Abstract

A suite of Ti-bearing garnets from magmatic, carbonatitic, and metamorphic rocks was studied by electron probe microanalysis (EPMA), X-ray powder diffraction (XRPD), single-crystal X-ray diffraction (SCXRD), Mössbauer spectroscopy, and secondary ion mass spectrometry (SIMS) to better characterize their crystal chemistry. The studied garnets show TiO_2 varying in the range of 4.9(1) to 17.1(2) wt% and variable $Fe^{3+}/\Sigma Fe$ content. SIMS analyses allowed quantification of light elements yielding H_2O in the range 0.091(7)–0.46(4), F in the range 0.004(1)–0.040(4), and Li_2O in the range 0.0038(2)–0.014(2) wt%. Mössbauer analysis provided spectra with different complexity, which could be fitted to several components variable from one ($^{Y}Fe^{3+}$) to four ($^{Y}Fe^{2+}$, $^{Z}Fe^{2+}$, $^{Y}Fe^{3+}$, $^{Z}Fe^{3+}$). A good correlation was found between the $Fe^{3+}/\Sigma Fe$ resulting from the Mössbauer analysis and that derived from the Flank method.

X-ray powder analysis revealed that the studied samples are a mixture of different garnet phases with very close cubic unit-cell parameters as recently found by other authors. Single-crystal X-ray refinement using anisotropic displacement parameters were performed in the $Ia\bar{3}d$ space group and converged to $1.65 \leq R_1 \leq 2.09\%$ and $2.35 \leq wR_2 \leq 3.02\%$. Unit-cell parameters vary in the range $12.0641(1) \leq a \leq 12.1447(1)$ Å, reflecting different Ti contents and extent of substitutions at tetrahedral site.

The main substitution mechanisms affecting the studied garnets are: $^{Y}R^{4+} + {}^{Z}R^{3+} \leftrightarrow {}^{Z}Si + {}^{Y}R^{3+}$ (schorlomite substitution); $^{Y}R^{2+} + {}^{Z}R^{4+} \leftrightarrow 2{}^{Y}R^{3+}$ (morimotoite substitution); $^{Y}R^{3+} \leftrightarrow {}^{Y}Fe^{3+}$ (andradite substitution); in the above substitutions $^{Y}R^{2+} = Fe^{2+}$, Mg^{2+}, Mn^{2+}; $^{Z}R^{4+} = Ti$; $^{Y}R^{3+} = Fe^{3+}$, Al^{3+}, Cr^{3+}; $^{Z}R^{3+} = Fe^{3+}$, Al^{3+}. Minor substitutions, such as $2{}^{Y}Ti^{4+} + {}^{Z}Fe^{2+} \leftrightarrow 2{}^{Y}Fe^{3+} + {}^{Z}Si$, $(SiO_4)^{4-} \leftrightarrow (O_4H_4)^{4-}$, $F^- \leftrightarrow OH^-$, and $^{Y}R^{4+} + {}^{X}R^{+} \leftrightarrow {}^{Y}R^{3+} + {}^{X}Ca^{2+}$, with $^{Y}R^{4+} = Ti$, Zr; $^{Y}R^{3+} = Fe^{3+}$, Al, Cr^{3+}; $^{X}R^{+} = Na$, Li also occur.

Keywords: Ti-bearing garnets, light elements, SCXRD, XRPD, EPMA, SIMS, Mössbauer spectroscopy, crystal chemistry

stituting cations over the three independent crystallographic sites and, with particular regards to Ti-rich garnets, of the multiple oxidation states and coordination environments of transition elements such as Fe and Ti. This topic has been thoroughly reviewed by Grew et al. (2013), also in view of the relevant implications for classification and nomenclature of garnets.

Ti-garnets may also incorporate hydrogen, fluorine, and lithium in trace but measurable amounts. In particular, the OH-bearing garnets may be a reservoir of hydrogen in the Earth's mantle and may also affect the evolution of the hydrosphere through its influence on mantle melting and isotopic fractionation (Bell et al. 2004).

Quantitative analysis of trace hydrogen is therefore necessary for a better understanding of its role in geological processes but, unfortunately, there is no routine method to obtain this information. For instance, the hydrogen content (conventionally quantified as H_2O, wt%) in schorlomites and Ti-andradites was often estimated from the summed integrated OH^- absorbance in the infrared spectra using a wavenumber-dependent calibration (Lager et al. 1989; Müntener and Hermann 1994; Locock et al. 1995; Amthauer and Rossman 1998; Katerinopoulou et al. 2009; Phichaikamjornwut et al. 2011). Actually, it has been demonstrated that the choice of a calibration method for garnets is not unambiguous since considerable discrepancies exists among the available calibrations (e.g., Maldener et al. 2003). The hydrogen content of titanian andradites from Sanbagawa metamorphic rocks (Central Japan), melilitic rocks of the Osečná complex (Bohemia), and schorlomites from Afrikanda (Kola Peninsula) silicocarbonatite was measured, respectively, by means of wet analysis, gravimetry, and combustion (Onuki et al. 1982; Ulrych et al. 1994; Chakhmouradian and McCammon 2005). Kühberger et al. (1989) used the solid's moisture analyzer to determine the water content in synthetic Ti-andradite.

Multiple mechanisms have been proposed to describe the hydrogen uptake in garnets. The hydrogarnet substitution ($4H + {}^{Z}\square \rightarrow \square + {}^{Z}Si$), where, i.e., a SiO_4 unit may be replaced by H_4O_4 on the tetrahedral site, was often invoked because consistent with diffraction technique data from H-rich samples (e.g., Lager et al. 1987, 1989; Eeckhout et al. 2002; Ferro et al. 2003). Evidences from electron microprobe data, nuclear magnetic resonance (NMR), and infrared (IR) spectra have been reported as pointing to octahedral and dodecahedral hydrogen occupancy in garnets (Basso et al. 1984a, 1984b; Kalinichenko et al. 1987; Basso and Cabella 1990; Rossman and Aines 1991).

Fluorine content of Ti-andradites or titanium andradites-grossular was mainly obtained by electron-microprobe analysis (Flohr and Ross 1989; Manning and Bird 1990; Barbanson and Bastos Neto 1992; Visser 1993; Ulrych et al. 1994; Freiberger et al. 2001; Faryad and Dianiška 2003) but also by F-sensitive glass electrode (Armbruster et al. 1998). Exchange reaction $F^- \leftrightarrow OH^-$ was used to explain the incorporation of fluorine in garnet, but also more complex reactions were proposed involving coupled cations substitutions for charge balance (Valley et al. 1983).

To the best of our knowledge, studies on lithium in Ti-garnets, instead, are missing in literature. For natural or synthetic Ti-free, Li-rich garnets it was proposed that lithium occupies not only the Z but also the Y, X, and interstitial 96*h* sites (Cussen 2006; Cempírek et al. 2010). These garnets have high-ionic conductivity (e.g., Wang and Lai 2012) or notable implications as a geobarometer (Yang et al. 2009).

In the present study, hydrogen, fluorine, and lithium were measured in a suite of Ti-garnets from various rock types by means of secondary ion mass spectrometry (SIMS). This technique was only previously used to derive an H_2O calibration curve employing, however, garnets with pyralspite composition, whose hydrogen abundance were determined by manometry and IR measurements (Koga et al. 2003).

The results of SIMS, electron microprobe analysis (EPMA), X-ray powder diffraction (XRPD), single-crystal X-ray diffraction (SCXRD), and Mössbauer spectroscopy have been integrated in the present study of Ti garnets of different origin and provenance to provide a comprehensive crystal chemical characterization of the studied samples.

Materials and methods

Samples

The analyzed samples are from different geologic environments: magmatic alkaline, carbonatitic, and metamorphic rocks. The details of samples origin and provenance are reported in Table 1. Most of the analyzed samples have been previously partially characterized and the relevant results published in the papers reported in the last column of Table 1. In the present work, for the first time a full crystal chemical characterization is accomplished for W6 and W16 samples. In addition, a re-examination of the crystal-chemical formulas of W12, NZALA, and ZER2 samples, previously studied by some of the authors, is here proposed on the basis of EPMA, SIMS, XRPD, and SCXRD measurements on new crystals. Non-routine chemical analysis (EPMA with the Flank method, SIMS see below) is reported for the first time on the whole suite of study samples as well as the results of XRPD measurements.

EPMA

Quantitative elemental analyses of the studied crystals (embedded in epoxy resin and polished) were performed with a JEOL JXA-8200 electron microprobe (Dipartimento di Scienze della Terra, University of Milano) operating at 15 kV acceleration voltage, 5 nA beam current, ~1 μm beam size, and 30 s counting time. All the elements were analysed in wavelength-dispersive spectrometry (WDS) mode and the adopted standards were: wollastonite (Si), anorthite (Al, Ca), olivine (Mg), fayalite (Fe), omphacite (Na), ilmenite (Ti), Cr pure (Cr), rhodonite (Mn), and zircon jarosite (Zr). A Phi-Rho-Z routine as implemented in the JEOL suite of programs was used for the matrix correction. Analytical measurements were affected by a relative uncertainty of 1% for major elements and 4% for minor elements. "Flank method" measurements for the determination of the $Fe^{3+}/\Sigma Fe$ were carried out with the same electron microprobe as above, in WDS mode, employing a TAP crystal and a 300 μm slit. Fe$L\beta$ and Fe$L\alpha$ peaks were searched and measured for counting times of 300 s. The correction for self-absorption was applied (Höfer and Brey 2007) and natural and synthetic garnet end-members with fixed $Fe^{3+}/\Sigma Fe$ were used as standards (Malaspina et al. 2009). The accuracy of the Flank method has been defined by a maximum error of ±0.04 for $Fe^{3+}/\Sigma Fe$ in samples with total Fe in the range 8–11wt% (Höfer and Brey 2007).

Table 1. Origin, provenance, and literature data of the analyzed samples

Label	Provenance	References
	Magmatic alkaline rocks	
W6	Iivaara, Finland	Howie and Woolley (1968)
W16	Rusinga Island, Kenya	Howie and Woolley (1968)
	Carbonatitic rocks	
W12	Magnet Cove, Arkansas	Howie and Woolley (1968); Pedrazzi et al. (2002)
	Metamorphic rocks	
NZALA	Atlas mountains, Marocco	Armbruster et al. (1998); Pedrazzi et al. (2002)
ZER2	Zermatt, Switzerland	Armbruster et al. (1998); Pedrazzi et al. (2002)

SIMS

SIMS analyses were performed with the ion microprobe Cameca IMS 4f installed at CNR-IGG (Pavia) following procedures similar to those reported in Ottolini et al. (1995, 2002). A static, mass filtered $^{16}O^-$ primary beam accelerated to 12.5 kV was focused on the sample surface to obtain a current intensity of 9.5 nA, corresponding to ~15 μm beam diameter. The second aperture (400 μm Ø) on the primary-beam selector was used to prevent $^{16}O^1H^-$ ions, which forms a weak second spot on the sample (clearly visible in anhydrous samples), from reaching the ion probe sample chamber (SC). Positive secondary ions from the sample were extracted by a 4.5 kV accelerating voltage and transferred into the mass spectrometer by the 25 μm secondary-ion optics. Secondary ions were "energy filtered" with an emission energy in the range ~75–125 eV. H^+, $^7Li^+$, $^{19}F^+$, and $^{30}Si^+$ ion signals were detected after 450 s waiting time required to get steady-state sputtering conditions. Acquisition times were 3 s for H^+ and $^7Li^+$ each, 8 s for $^{19}F^+$, and 3 s for $^{30}Si^+$ for each of the two analytical cycles. Hydrogarnet crystals and standards were left to degas seven days in the ion probe SC before running analysis. Detection limits for H (6σ background) were estimated on the order of 20 ppm H.

The results for H, Li, and F were put on a quantitative basis using empirical calibration curves based on standards that were the following: schorl (no. 16), dravite (no. 18), elbaite (no. 19), fully characterized in Ottolini et al. (2002). In particular, for H quantification we used the extrapolated regression line: IY(H/Si) vs. (Fe_{tot}+Ti+Mn)(at), first derived in kornerupine (Ottolini and Hawthorne 2001) and then successfully tested in several silicate matrixes (see for instance, Scordari et al. 2010 and reference therein). The analytical accuracy for Li is on the order of 5% relative. An accuracy of better than 10% relative is quoted for H and F.

Mössbauer spectroscopy

Mössbauer spectra were recorded on powdered samples (~10 mg) at room temperature, in transmission geometry, using a source of ^{57}Co/Rh matrix (~1 GBq) and a constant acceleration spectrometer. Spectra were recorded using a multichannel analyzer (1024 or 512 channels) in the velocity range ±4 mm/s and subsequently folded (Shenoy et al. 1978). More than 10×10^6 baseline counts per channel were recorded for each spectrum. Isomer shifts (IS) are expressed relative to α-iron. The spectra were fitted with routines employing Levemberg-Marquardt methods and implemented in the software RECOIL 1.03a (Lagarec and Rancourt 1997, 1998).

XRPD

X-ray powder diffraction patterns were recorded using a PANalytical Empyrean diffractometer equipped with a PIXcel-3D detector. Cu*K*α radiation (λ = 1.5418 Å) was employed and the instrument operated at 40 kV/40 mA. Because of the shortage of samples, powders were loaded in a zero background silicon sample holder and slightly compressed with a glass slide. The patterns were collected in the 2θ range of 5–140°. The divergence and antiscatter slits were 1/8 and ¼ mm, respectively, and the detector slit was 7.5 mm. Qualitative phase analysis was performed by means of the PANalytical HighScore software. Quantitative analysis and the refinement of the lattice parameters were carried out by the Rietveld Method (Young 1993) as implemented in the GSASII software (Toby and Von Dreele 2013).

SCXRD

Single-crystal X-ray diffraction data were collected using a Bruker AXS X8 APEXII automated diffractometer (Dipartimento di Scienze della Terra e Geoambientali, University of Bari) with a charge coupled device (CCD) detector and a four-circle Kappa goniometer. The X-ray data were acquired using a graphite monochromatized Mo*K*α radiation, several ω and φ rotation scans, 1.0° scan width, 10 s per frame exposure time, crystal-to-detector distance of 40 mm, and operating conditions of 50 kV and 30 mA. The COSMO program of the Apex program suite (Bruker 2003a) was used to optimize the data collection strategy, whereas for cell determination and data reduction the SAINT (Bruker 2003b) and SADABS programs (Sheldrick 2003) were employed. Least-squares refinements were performed using the program CRYSTALS (Betteridge et al. 2003) in the space group $Ia\bar{3}d$. Scale factor, atomic positions, cation occupancies, and anisotropic displacement factors were refined. Fully ionized scattering factors were used. Since compositional disorder can affect all three independent sites in the garnet structure (see the Introduction section) different cation distribution were tested to obtain the best fit between mean atomic numbers estimated via EPMA and structure refinement (X-ref). Preliminary refinements allowed to ascertain that tetrahedral site occupancy could assume values less than 1, indicating the occurrence of tetrahedral vacancies. In addition, the refined tetrahedral mean atomic number could be less or greater than 14 e^-, indicating, respectively, the presence of a lighter or a heavier substituent of Si atoms. Also Ca occupancy was initially left free to vary to check for the occurrence of Fe^{2+} at X (in this case the mean atomic number would refine to more than 20 e^-). In final refinements, depending of the bulk chemistry of each sample, the following refinement restrictions (Watkin 2008) were used: (1) at the X-site, the occupancy of Ca was constrained so that the site was fully occupied; (2) at the Y-site, the Al and Fe occupancies [with Fe representing Mn + Ti (+Zr) and Al representing Mg scattering species] were restrained to obtain a full occupancy; and (3) at the Z-site, the Si (standing also for Al), or Si and Fe occupancies were refined with a restraint that could result in a total occupancy less, equal, or greater than 1.The only exception was for sample ZER2: in this case Si occupancy was constrained to be 1.

Results and discussion

Chemical composition

EPMA data calculated as average over 4–10 spots are reported in Table 2 together with SIMS data. Indeed, the within grain coefficient of variation (CV) is <10% for all the measured oxides with the exception of Na_2O, ZrO_2, Cr_2O_3, whereas as far as light elements are concerned, it is ~10% for H_2O, generally > 50% for Li_2O and variable (4–44%) for the F content.

In particular, the studied Ti-garnets are characterized by variable degree of hydration. SIMS analyses provide H_2O concentration in the range 0.091(7)–0.46(4) wt% (Table 2) which is in agreement (see also Fig. 1) with the values measured for most of the Ti-garnets with andradite, andradite-grossular, andradite-uvarovite, or schorlomite component (Müntener and Hermann 1994; Locock et al. 1995; Amthauer and Rossman 1998; Chakhmouradian and McCammon 2005; Katerinopoulou et al. 2009; Phichaikamjornwut et al. 2011). However, higher H_2O contents (from 1.25 to 2.90 wt%) were reported for other Ti-garnets (Onuki et al. 1982; Lager et al. 1989; Ulrych et al. 1994; Amthauer and Rossman 1998). Galuskin (2005) calculated, on the basis of charge balance, ~5 wt% H_2O in the "hydroschorlomite," whereas up to 10 wt% H_2O was estimated from cell dimensions considerations in the "hydroandradite" (Armbruster 1995).

Very low amount of Li_2O [0.0038(2)–0.014(2) wt%] equivalent to 0.001–0.005 atoms per formula unit (apfu) was detected in the studied samples (Table 2). These values are similar to those (0–0.004 apfu) found in Ti-free garnets (Grew et al. 1990). Cempírek et al. (2010) measured 0.019–0.079 Li pfu in almandine from leucocratic granulite of Czech Republic. For

Table 2. Chemical composition (wt%) of the studied garnets

	W6	W12	W16	NZALA	ZER2
CaO	31.7(1)	32.2(1)	31.5(1)	31.9(1)	33.2(1)
Na_2O	0.31(2)	0.05(3)	0.35(2)	0.14(2)	0.01(1)
MgO	1.20(2)	0.99(1)	0.95(3)	0.75(2)	0.44(3)
MnO	0.21(2)	0.26(3)	0.33(2)	0.51(2)	0.23(3)
FeO	19.3(2)	20.1(1)	19.7(2)	20.8(3)	20.9(2)
Al_2O_3	0.96(2)	2.08(4)	1.0(1)	1.17(4)	2.5(1)
ZrO_2	0.18(2)	0.01(1)	0.37(3)	0.2(1)	0.15(1)
TiO_2	17.1(2)	9.26(2)	15.7(1)	9.3(3)	4.9(1)
Cr_2O_3	0.02(1)	0.02(2)	0.01(1)	0.07(3)	0.13(4)
SiO_2	27.0(1)	29.9(1)	27.9(1)	30.4(2)	34.5(4)
Total	98.0(2)	94.9(3)	97.8(2)	95.2(4)	97.0(4)
H_2O^a	0.31(3)	0.17(1)	0.22(3)	0.091(7)	0.46(4)
Li_2O^a	0.004(2)	0.0038(2)	0.011(6)	0.008(1)	0.014(2)
F^a	0.009(4)	0.011(2)	0.040(4)	0.020(1)	0.004(1)
$Fe^{3+}/\Sigma Fe^b$	0.90(1)	0.96(1)	0.88(2)	0.92(1)	1.00(1)
$Fe^{3+}/\Sigma Fe^c$	0.79	0.96	0.79	0.92	0.86

[a] SIMS data.
[b] From Flank method.
[c] Calculated on the basis of the charge balance according to Grew et al. (2013) (see details in the text).

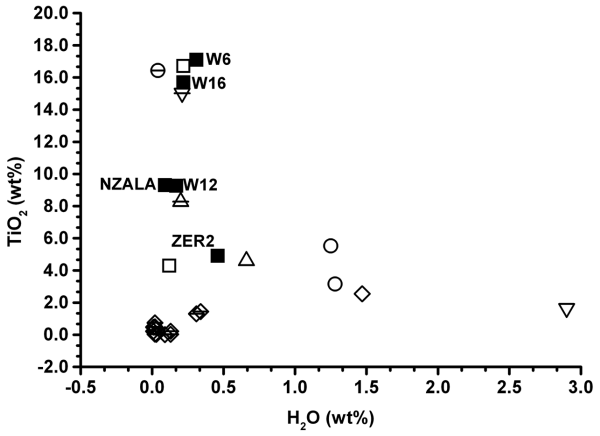

FIGURE 1. Plot of the TiO_2 (wt%) vs. measured H_2O (wt%) in Ti-garnets. Symbols: solid squares = samples of this work; open symbols = samples from literature; circle = 80802 and 80303 from Onuki et al. (1982); pointing downward triangle = SB-3 from Lager et al. (1989); pointing upward triangle = SA12 from Müntener and Hermann (1994); diamond = 31/B from Ulrych et al. (1994); circle with horizontal line = Ice River crystal from Locock et al. (1995); pointing downward triangle with horizontal line = AF-05 from Chakhmouradian and McCammon (2005); pointing upward triangle with horizontal line = M-1 from Katerinopoulou et al. (2009); diamond with horizontal line = KPK39-1-1, KPK54-10, KPK54-11, KTK05, KTK07, KTK09, KTK10, KPK56-12-2, KPK56-12-9, KPN09, KPN10, and KPN11 from Phichaikamjornwut et al. (2011).

synthetic Li-rich majoritic garnet, Yang et al. (2009) provide 1.96 Li pfu, whereas up to about 7 Li atoms pfu were reported for other synthetic garnets (Wang and Lai 2012). This element occurs as a major chemical component in the garnet end-member cryolithionite, $Na_3Al_2Li_3F_{12}$ (Geller 1971).

Regarding the fluorine concentration, in our samples it ranges from 0.004(1) to 0.040(4) wt% (Table 2), which corresponds to 0.001–0.010 apfu. Literature data indicate F content ranging from ~0.1 to 5 wt% in Ti-garnets with andradite and andradite-grossular component (Flohr and Ross 1989; Manning and Bird 1990; Barbanson and Bastos Neto 1992; Visser 1993; Ulrych et al. 1994; Armbruster et al. 1998; Freiberger et al. 2001; Faryad and Dianiška 2003) and is equal to ~6 wt% in the F-rich hibschite (Chakhmouradian et al. 2008), showing that in our garnets all values are on the lower end of the natural variability interval.

Iron speciation

The iron oxidation state was determined both via electron microprobe analysis [the Flank method (Höfer and Brey 2007)] and Mössbauer spectroscopy. Specifically, the Flank method was used on the same single crystals that underwent structure refinement, whereas Mössbauer analyses were carried out on powders of the W6 and W16 samples. The results are reported, respectively, in Tables 2 and 3. Mössbauer spectra of samples W6 and W16 are in Figures 2a and 2b, whereas comparison between Mössbauer and Flank method is in Figure 3. In Table 3 Mössbauer data on W12, NZALA, and ZER2 samples from previous work (Pedrazzi et al. 2002) are also reported for comparison. The fitting of the room-temperature Mössbauer spectra (Fig. 2) allowed to identify different iron species: $^{Y}Fe^{3+}$, $^{Z}Fe^{3+}$, $^{Z}Fe^{2+}$, and $^{Y}Fe^{2+}$. The assignment and the values of the hyperfine parameters (Table 3) are in agreement with the results of previous investigations on Ti-garnets (Ortalli et al. 1994; Pedrazzi et al. 1998, 2002; Scordari et al. 1999; Schingaro et al. 2004; Dyar et al. 2012). In particular, the $^{Z}Fe^{2+}$ species has been reported in other Mössbauer spectra on Ti-garnets (Kühberger et al. 1989; Locock et al. 1995; Chakhmouradian and McCammon 2005), but its interpretation is still uncertain and, recently, Chakhmouradian and

TABLE 3. Mössbauer parameters of W6 and W16 garnets as obtained by Lorentzian fitting and corrected according to Dyar et al. (2012)

	χ^2_r	Site	Species	IS (mm/s)	QS (mm/s)	Γ (mm/s)	A(%)
		Y	Fe^{3+}	0.393(6)	0.64(1)	0.38(1)	70(1)
W6	0.93	Z	Fe^{3+}	0.20(1)	1.20(5)	0.32(4)	20(1)
		Z	Fe^{2+}	0.7(2)	1.7(7)	0.6(2)	10(2)
		Y	Fe^{3+}	0.402(4)	0.61(1)	0.37(8)	59(1)
		Y	Fe^{2+}	1.3(7)	2.8(3)	0.52(6)	10(2)
W16	1.40	Z	Fe^{3+}	0.22(1)	1.28(6)	0.37(3)	19(3)
		Z	Fe^{2+}	0.7(6)	1.6(8)	0.46(6)	12(2)
		Y	Fe^{3+}	0.399(5)	0.617(6)	0.326(5)	81(3)
W12[a]	1.29	Z	Fe^{3+}	0.221(2)	1.208(4)	0.401(4)	19(2)
		Y	Fe^{3+}	0.402(5)	0.597(5)	0.331(6)	79(7)
NZALA[a]	1.11	Z	Fe^{3+}	0.208(1)	1.253(3)	0.318(4)	12(7)
		Z	Fe^{2+}	0.70(1)	1.66(1)	0.25(9)	4(2)
		Y	Fe^{2+}	1.28(8)	2.91(2)	0.48(2)	5(3)
ZER2[a]	1.16	Y	Fe^{3+}	0.399(1)	0.582(3)	0.312(4)	100

Notes: χ^2_r = reduced χ^2 = χ^2/degrees of freedom. Literature data on W12, NZALA and ZER2 samples (Pedrazzi et al. 2002) are also reported.
[a]Data from Pedrazzi et al. (2002).

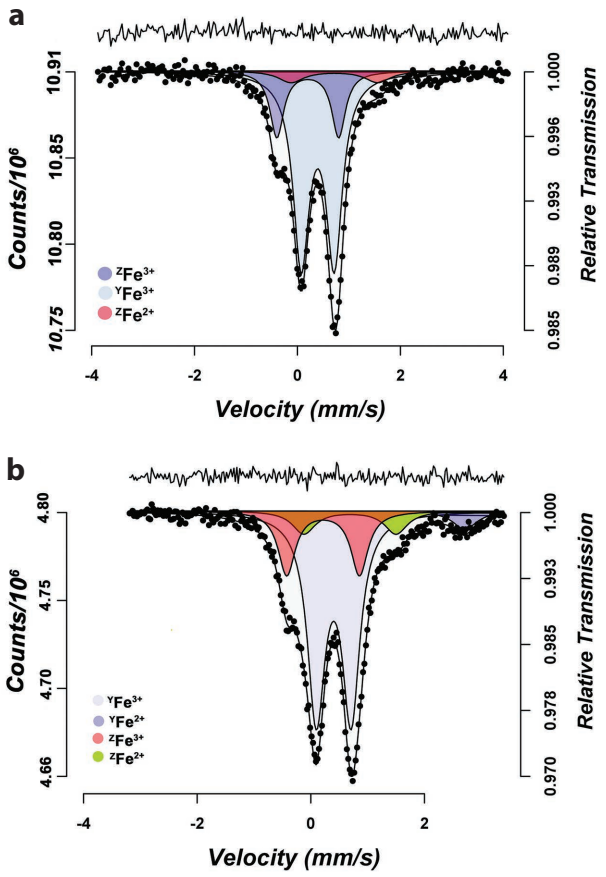

FIGURE 2. Room-temperature Mössbauer spectra of samples W6 (**a**) and W16 (**b**). (Color online.)

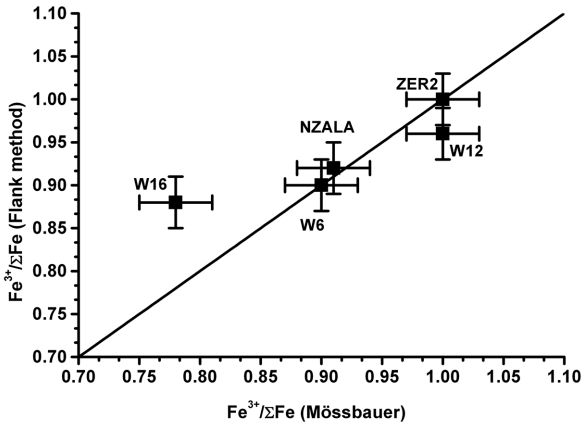

FIGURE 3. Comparison between $Fe^{3+}/\Sigma Fe$ as determined by Mössbauer spectroscopy and Flank method. The 1:1 line is shown. The error bars for $Fe^{3+}/\Sigma Fe$ correspond, respectively, to $\sigma = 3\%$ for the Flank method (Malaspina et al. 2012) and $\sigma = 3\%$, the latter being the maximum error for Mössbauer data (Dyar et al. 2008).

McCammon (2005) have reinterpreted this component as $^{Y}Fe^{2+} \leftrightarrow {}^{Z}Fe^{3+}$ electron transfer. However, attempts to fit the spectra of W6, W16, and NZALA samples according to the model 2 in Chakhmouradian and McCammon (2005) were unsuccessful.

The comparison between $Fe^{3+}/\Sigma Fe$ as measured by Mössbauer and Flank method derived (Fig. 3) indicates a good correlation ($R^2 \approx 0.8$) between the two sets of measurements. The observed discrepancies, specifically for the W12 and W16 samples, may be due to the crystal chemical heterogeneity of the sample, so that the single crystals selected for EPMA and SCXRD may be not representative of the powders (see also the section XRPD below).

Structural features

XRPD results. The X-ray powder diffraction analysis was performed on all the study samples (see the patterns in Fig. 4) with the exception of ZER2, whose amount was too scarce to be measured. The qualitative analysis evidenced that no phase impurity occurs. However, splitting or asymmetry of the diffraction peaks is observed, suggesting the presence in our powders of different garnet phases with similar unit-cell parameters (Fig. 5). Indeed in all samples, at least two cubic garnet phases

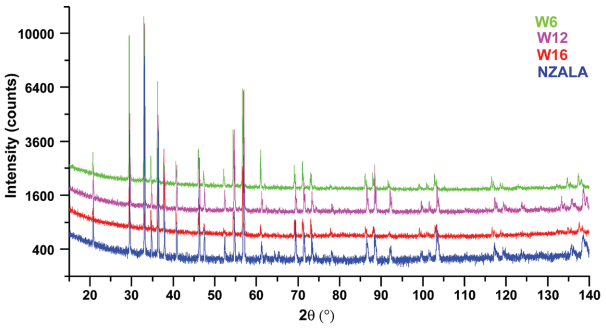

FIGURE 4. XRD patterns of the W6, W12, W16, and NZALA samples. (Color online.)

(labelled phase I and II on the basis of the relative abundances) were clearly distinguished and their weight fractions and cell parameters were refined using GSASII; the results are shown in Table 4. In the case of W6 and W16 samples, a third phase seems to be present (Fig. 5), but the attempts to refine it were unsuccessful. These results are in agreement with recent findings relevant to the study of optical anomalies in garnets. In particular, these studies have shown that both Ti-bearing and Ti-free garnets can actually be a mixture of two or more cubic phases with slightly different cell parameters and composition (Antao 2013, 2014; Antao and Klincker 2013; Antao and Round 2014). The consequent structural mismatch causes strain that results in low-to-strong degree of optical anisotropy (birefringence). In our case, the garnets appear not completely extinct upon observation under cross-polarized light, but did not show difference in chemical composition at least at the EPMA scale (see above). Similar results were reported for a Ti-andradite from Magnet Cove (Antao 2013). In brief, anomalous optical behavior is due to intergrowth of more than one cubic phase, that, if occurs at a fine scale, leads to homogeneous EPMA data, whereas at a large scale should be detected as a slight variation of chemical composition. To the best of our knowledge, it is the first time that a mixture of cubic phases has been detected for Ti-garnets with laboratory instrumentation. In addition, data in Table 4 show that the dominant phase of the mixture (phase I) has, in most cases, unit-cell parameters similar to those obtained from the relevant samples in SCXRD analysis (see below).

SCXRD results. The main results of SCXRD investigation, in particular about crystal data, data-collection parameters, and figures of merit on structure refinements, are also summarized in Table 4. Refined site positions, atomic occupancies, and anisotropic displacement parameters are listed in Table 5, whereas distances and distortional parameters are reported in Table 6. (CIF[1] is available.)

All structure refinements converged to good values of the discrepancy factors: $1.65 \le R_1 \le 2.09\%$ and $2.35 \le wR_2 \le 3.02\%$.

The cell-edges variation of the analyzed crystals (Table 4) reflects different Ti contents (Table 2), a correlation already pointed out by Howie and Woolley (1968). In particular, a positive trend of the *a* parameter vs. the TiO_2 content has been found (Fig. 6).

However, by inspection of Figure 7 it is evident that the *a*-cell parameter increment depends on the increase of both the <X-O> ($R^2 = 0.90$ in Fig. 7a) and Z-O ($R^2 = 0.86$ in Fig. 7c), whereas the dependence from the Y-O variation seems to be negligible ($R^2 = 0.004$ in Fig. 7b). Since the X-site composition is almost constant in the study samples (see Table 7), the increase of <X-O> is induced by the polyhedral edge-sharing (X/Z) occurring in the garnet structure.

From Table 6 it can be noticed that the Δ(X-O) and α values are in the range of variability for the known natural silicate garnets (Ungaretti et al. 1995; Yang et al. 2009). The tendency to the decrease of Δ(X-O) with increasing Fe^{3+} content along the grossular-andradite join (Ungaretti et al. 1995) is also present in our samples, where it appears also related to the Fe^{3+}+Ti content.

[1] Deposit item AM-16-25439, CIF. Deposit items are free to all readers and found on the MSA web site, via the specific issue's Table of Contents (go to http://www.minsocam.org/MSA/AmMin/TOC/).

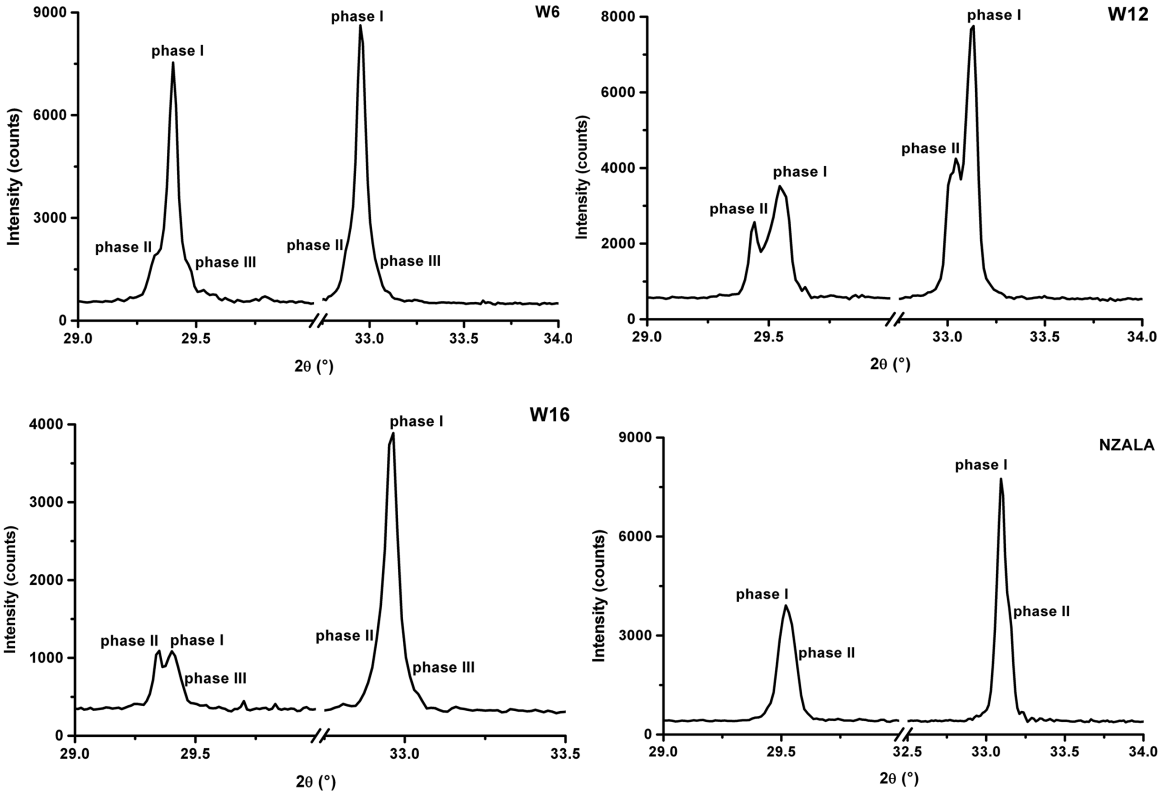

FIGURE 5. Splitting of selected diffraction peaks, (004) and (024), from the patterns in Figure 4.

Octahedral and tetrahedral sites in garnets are variously distorted, as evident from the analysis of octahedral angle variance and tetrahedral angle variance (OAV and TAV, Table 6), which quantifies the deviation from the ideal value of 90° and 109.47°, respectively, of the relevant polyhedra (Table 6, Figs. 8 and 9). In particular, the tetrahedron is the most distorted polyhedron in garnets and the distortion increases with increasing the $^{Z}(Fe^{2+}+Al+Fe^{3+}+Ti)$ content (Fig. 8). On the other hand, since each tetrahedron in the garnet structure shares edges with two dodecahedra, the shared O-O tetrahedral edges, S(Z), are always shorter than the unshared ones, U(Z) and, at the same time, the tetrahedron is elongated along the $\overline{4}$ axis (see t_{SZ}, the distance between shared edges in Table 6) for a better screening of the repulsive interaction between the X and Z cations. The octahedron is most distorted in grossular and becomes more regular with the entrance of high charge cations or of trivalent cations different from Al^{3+} (Fig. 9). In addition, substitutions at Y affect the t_{SY} parameter in that, starting from pure grossular, where the octahedron is flattened along the $\overline{3}$ axis, if a cation larger than Al occurs at Y the octahedron tends to elongate along the same axis, as also observed by other authors (Ungaretti et al. 1995).

The ZER2 sample has bond distances and distortion parameters very similar to that of pure andradite (Adamo et al. 2011). For instance, for this sample the <D-O> parameter (2.131 Å) is identical to that of the pure andradite (2.132 Å, Adamo et al. 2011) and is a consequence of its short Z-O distance (Table 6), indicating a low extent of substitution at the Z site. The increase in the Z-O distances in the other samples accounts for a greater extent of schorlomitic and hydrogarnet substitutions. These features entail the increase of the <D-O> parameters up to values close to that (2.186 Å) of kimzeyite of Schingaro et al. (2001), see Table 6.

Crystal chemical formulas

Grew et al. (2013) suggested a procedure to perform a cation distribution for Ti-garnets basing only on chemical data; the results obtained using their spreadsheet are reported in Table 7. In the same table we also reported the structural formulas of the study garnets, obtained using a multimethodic approach adopted in the present work. Specifically, they were calculated combining the EPMA-SIMS data with the Mössbauer results. The latter were considered representative of the single crystals. This assumption is generally sensible, on the basis of the Flank method analysis (see above). From the two sets of crystal chemical formulas, mean atomic numbers as well as bond distances using ionic radii from Shannon (1976) have been calculated. These values are shown in Table 8 where they are compared with those derived from the structure refinement.

Samples W12 and ZER2 contain the smallest number of Fe species ($^{Y}Fe^{3+}$, $^{Z}Fe^{3+}$ the former and only $^{Y}Fe^{3+}$ the latter, see Table 3) and in particular ZER2 has the simplest composition among the whole suite here considered. Comparison to the formulas derived through the approach devised by Grew et al. (2013) indicates that charge balance tends to overestimate the

TABLE 4. Powder and single-crystal X-ray diffraction data of the studied garnets

	W6		W12		W16		NZALA		ZER2
XRPD data									
	phase I	phase II	phase I	phase II	phase I	phase II	phase I	phase II	
Weight fraction (%)	66(3)	34(3)	58(2)	42(2)	81(2)	19(2)	80(2)	20(1)	
a (Å)	12.1476(2)	12.1599(9)	12.0948(3)	12.1156(7)	12.1459(2)	12.1648(9)	12.1045(2)	12.0883(3)	
N_{obs}	148	148	146	148	148	148	148	146	
Data points	10383		10383		10383		10383		
wR (%)	10.45		11.54		10.49		10.12		
SCXRD data									
Crystal size (mm³)	0.60 × 0.58 × 0.23		0.48 × 0.24 × 0.16		0.56 × 0.33 × 0.07		0.60 × 0.50 × 0.14		0.51 × 0.22 × 0.11
Space group	*Ia*$\bar{3}$*d*		*Ia*$\bar{3}$*d*		*Ia*$\bar{3}$*d*		*Ia*$\bar{3}$*d*		*Ia*$\bar{3}$*d*
a (Å)	12.1447(1)		12.1039(1)		12.1411(1)		12.0869(2)		12.0641(1)
Cell volume (Å³)	1791.27(3)		1773.27(3)		1789.67(3)		1765.81(5)		1755.84(3)
Z	8		8		8		8		8
θ range for data collection	4 to 36°		5 to 30°		4 to 36°		5 to 36°		4 to 36°
Reflections collected	20828		14993		20821		20402		20641
Reflections unique	366		228		366		363		362
$R_{merging}$ (R_{int}) (%)	2.20		2.20		1.93		3.47		1.77
Reflections used [$I > 3\sigma(I)$]	332		206		341		323		334
No. of refined parameters	21		21		21		21		19
Goof[c]	1.08		0.92		1.02		0.94		0.87
R_1[a] (on *F*) (%)	2.00		1.78		1.95		1.65		2.09
wR_2[b] (on F^2) (%)	2.94		2.38		2.55		2.35		3.02
$\Delta\rho_{min}/\Delta\rho_{max}$ ($e^-/Å^3$)	–0.40/0.49		–0.74/0.25		–0.40/0.49		–0.43/0.36		–0.96/0.34

[a] $R_1 = \Sigma[|F_o| - |F_c|]/\Sigma|F_o|$.
[b] $wR_2 = [\Sigma[w(F_o^2 - F_c^2)^2]/\Sigma[w(F_o^2)^2]]^{1/2}$; w = quasi-unit weight.
[c] Goodness-of-fit = $[\Sigma[w(F_o^2 - F_c^2)^2]/(N - p)]^{1/2}$, where N and p are the number of reflections and parameters, respectively.

TABLE 5. Crystallographic coordinates, site occupancies, equivalent/isotropic (Å²), and anisotropic displacement parameters (Å²) of the studied crystals

Sample	Site	Atom	*x*	*y*	*z*	Occ.	$U_{iso/equiv}$	U_{11}	U_{22}	U_{33}	U_{23}	U_{13}	U_{12}
W6													
	X	Ca^{2+}	1/8	0	1/4	1.0000	0.0087	0.0063(2)	0.0099(1)	0.0099(1)	0.00252(8)	0	0
	Y	Fe^{3+}	0	0	0	0.7304(8)	0.0049	0.0049(1)	0.0049(1)	0.0049(1)	0.00038(4)	0.00038(4)	0.00038(4)
		Al^{3+}				0.2698(8)							
	Z	Si^{4+}	3/8	0	1/4	0.878(1)	0.0054	0.0046(2)	0.0059(2)	0.0059(2)	0	0	0
		Fe^{3+}				0.137(5)							
	O	O^{2-}	0.03779(5)	0.04819(5)	0.65358(5)	1.0000	0.0102	0.0132(3)	0.0088(2)	0.0085(2)	–0.0010(2)	0.0031(2)	–0.0016(2)
W12													
	X	Ca^{2+}	1/8	0	1/4	1.0000	0.0078	0.0058(2)	0.0088(2)	0.0088(2)	0.00214(9)	0	0
	Y	Fe^{3+}	0	0	0	0.732(1)	0.0044	0.0044(2)	0.0044(2)	0.0044(2)	0.00009(5)	0.00009(5)	0.00009(5)
		Al^{3+}				0.268(1)							
	Z	Si^{4+}	3/8	0	1/4	0.935(2)	0.0041	0.0038(3)	0.0043(3)	0.0043(3)	0	0	0
		Fe^{3+}				0.064(1)							
	O	O^{2-}	0.03825(4)	0.04823(4)	0.65400(4)	1.0000	0.0078	0.0096(3)	0.0073(3)	0.0066(3)	–0.0002(2)	0.0018(2)	–0.0007(2)
W16													
	X	Ca^{2+}	1/8	0	1/4	1.0000	0.0085	0.0059(1)	0.0099 (1)	0.0099 (1)	0.00279(9)	0	0
	Y	Fe^{3+}	0	0	0	0.728(1)	0.0045	0.0045(1)	0.0045(1)	0.0045(1)	0.00049(5)	0.00049(5)	0.00049(5)
		Al^{3+}				0.272(1)							
	Z	Si^{4+}	3/8	0	1/4	0.859(1)	0.0052	0.0042(2)	0.0057(2)	0.0057(2)	0	0	0
		Fe^{3+}				0.143(5)							
	O	O^{2-}	0.03793(5)	0.04821(5)	0.65372(5)	1.0000	0.0099	0.0130(3)	0.0087(3)	0.0080(2)	–0.0008(2)	0.0028(2)	–0.0017(2)
NZALA													
	X	Ca^{2+}	1/8	0	1/4	1.0000	0.0083	0.0062(1)	0.0094(1)	0.0094(1)	0.00202(6)	0	0
	Y	Fe^{3+}	0	0	0	0.7932(9)	0.0050	0.0050(1)	0.0050(1)	0.0050(1)	0.00015(3)	0.00015(3)	0.00015(3)
		Al^{3+}				0.207(1)							
	Z	Si^{4+}	3/8	0	1/4	0.912(1)	0.0052	0.0045(2)	0.0055(2)	0.0055(2)	0	0	0
		Fe^{3+}				0.071(5)							
	O	O^{2-}	0.03869(4)	0.04831(4)	0.65454(4)	1.0000	0.0085	0.0098(2)	0.0084(2)	0.0072(2)	–0.0001(1)	0.0010(1)	–0.0004(1)
ZER2													
	X	Ca^{2+}	1/8	0	1/4	1.0000	0.0064	0.0046(2)	0.0074(1)	0.0074(1)	0.00170(7)	0	0
	Y	Fe^{3+}	0	0	0	0.792(1)	0.0046	0.0046(2)	0.0046(2)	0.0046(2)	0.00006(4)	0.00006(4)	0.00006(4)
		Al^{3+}				0.208(1)							
	Z	Si^{4+}	3/8	0	1/4	1.0000	0.0049	0.0043(2)	0.0052(2)	0.0052(2)	0	0	0
	O	O^{2-}	0.03899(4)	0.04825(4)	0.65457(4)	1.0000	0.0064	0.0070(2)	0.0067(2)	0.0055(2)	–0.0000(2)	0.0004(2)	–0.0002(2)

$^{Y}Fe^{2+}$ specie. For example, for the ZER2 garnet, both the Flank method and Mössbauer analysis provide $Fe^{3+}/\Sigma Fe = 100\%$, whereas from Grew et al. (2013) $Fe^{3+}/\Sigma Fe = 86\%$ is estimated (see Tables 2, 3,7 and Fig. 3). Comparison to the crystallographic data (Table 8) shows that a better agreement is obtained with our multi-methodic approach for the Y site, that allows a better modeling of this site in terms of mean atomic number as well as bond distances. In particular good agreement is found between the Y-O distance derived from the X-ray refinement (Y-$O_{X\text{-}ref}$) and that calculated from the EPMA (Y-O_{EPMA*}) with Δ = (Y-$O_{X\text{-}ref}$) – (Y-O_{EPMA*}) = 0.008 Å (see Table 8). On the contrary, if the approach in Grew et al. (2013) is used, Δ increases to 0.021 Å. Note that the use of the directly measured iron speciation implies that the Y site hosts significant amount of Ti^{3+}, as pre-

TABLE 6. Refined bond distances (Å) and distortional parameters of the studied samples, selected literature Ti-garnets and natural end-member garnets

	W6	W12	W16	NZALA	ZER2	Ti-andradite Lager et al. (1989)	Ti-andradite Müntener and Hermann (1994)	Ti-Zr-Cr-rich andradite Katerinopoulou et al. (2009)
X1-O	2.371(1)	2.366(1)	2.371(1)	2.364(1)	2.362(1)	2.369(1)	2.365(1)	2.361(1)
X2-O	2.518(1)	2.510(1)	2.517(1)	2.508(1)	2.505(1)	2.508(1)	2.512(1)	2.510(1)
<X-O>	2.445(1)	2.438(1)	2.444(1)	2.436(1)	2.434(1)	2.439(1)	2.439(1)	2.436(1)
Y-O	2.008(1)	2.008(1)	2.010(1)	2.0121(4)	2.009(1)	2.015(1)	2.014(1)	1.999(1)
Z-O	1.684(1)	1.671(1)	1.681(1)	1.6615(4)	1.656(1)	1.666(1)	1.658(1)	1.670(1)
<D-O> (Å)	2.145	2.139	2.145	2.136	2.131	2.140	2.137	2.135
V_X (Å^3)	25.019	24.759	25.001	24.705	24.616	24.781	24.790	24.731
Δ(X-O)	0.147	0.138	0.145	0.143	0.137	0.139	0.146	0.149
α (°)	26.518	26.851	26.603	26.888	26.847	26.950	26.771	26.429
V_Y (Å^3)	10.786	10.816	10.818	10.873	10.791	10.904	10.885	10.652
OAV (°^{2})	0.259	0.47	0.329	0.705	0.973	0.579	0.969	0.580
S(Y) (Å)	2.851	2.858	2.855	2.867	2.863	2.868	2.871	2.845
U(Y) (Å)	2.827	2.825	2.828	2.827	2.816	2.831	2.824	2.809
t_{SY} (Å)	2.298	2.294	2.298	2.292	2.280	2.297	2.287	2.279
t_{UY} (Å)	2.338	2.347	2.343	2.357	2.357	2.356	2.363	2.338
X-Y (Å)	3.395	3.383	3.394	3.378	3.372	3.384	3.379	3.377
φ(°)	133.55	133.42	133.53	133.49	133.64	133.39	133.70	133.81
V_Z (Å^3)	2.42	2.368	2.408	2.324	2.31	2.348	2.312	2.358
TAV (°^{2})	33.847	30.567	32.915	31.801	29.135	31.102	31.803	32.615
S(Z) (Å)	2.618	2.605	2.615	2.587	2.586	2.596	2.582	2.598
U(Z) (Å)	2.813	2.789	2.807	2.773	2.764	2.781	2.768	2.788
t_{SZ} (Å)	2.118	2.094	2.112	2.085	2.073	2.089	2.081	2.097
t_{UZ} (Å)	1.851	1.842	1.849	1.829	1.828	1.836	1.826	1.837
X-Z (Å)	3.036	3.026	3.035	3.022	3.016	3.027	3.022	3.020

Notes: <D-O> = [(Z-O) + (Y-O) + (X1-O) + (X2-O)]/4 according to Antao (2013); Volume of X, Y, and Z sites calculated using the IVTON software (Balić-Žunić and Vicković 1996); Δ(X-O) = (X2-O) – (X1-O) (Ungaretti et al. 1995); α: tetrahedral rotation along the $\bar{4}$ axis (Born and Zemann 1964); TAV and OAV: tetrahedral and octahedral, respectively, angle variance (Robinson et al. 1971); S(Y) and S(Z) stand for shared edges of octahedra and tetrahedra, respectively; U(Y) and U(Z) stand for unshared edges of octahedra and tetrahedra, respectively; t_{SY} and t_{SZ}: the distance between shared edges of octahedra and tetrahedra, respectively; t_{UY} and t_{UZ}: the distance between unshared edges of octahedra and tetrahedra, respectively; X-Y and X-Z: interatomic distance between the X cation and Y and Z cation, respectively; φ: Si-O-Y angle (Yang et al. 2009).

(Table extends on next page)

viously found in the Val Malenco Ti-bearing garnets (Müntener and Hermann 1994; 175, 274, 275, 276 crystals in Merli et al. 1995). As found for the sample ZER2, also in sample W12 $^{Y}Fe^{2+}$ is overestimated, since Mössbauer spectrum only shows Fe^{3+} species (Tables 2 and 3) and our formula, as before, provides a better modeling of the octahedral site.

In the case of sample W6 the Mössbauer spectrum is more complex and in particular the $^{Z}Fe^{2+}$ species has been detected. Although controversial (Chakhmouradian and McCammon 2005) this species is taken into account by Grew et al. (2013) in the procedure for site allocation of cations in Ti-garnets. However, the substitution explaining the $^{Z}Fe^{2+}$ uptake in the garnet structure is not specified. In the literature two mechanisms have been proposed for the charge balance in this case: $^{Z}Si^{4+} + 2O^{2-} \leftrightarrow {}^{Z}R^{2+} + 2(OH)^{-}$ (Kühberger et al. 1989) and $2\,^{Y}Ti^{4+} + {}^{Z}Fe^{2+} \leftrightarrow 2\,^{Y}Fe^{3+} + {}^{Z}Si$ (Locock et al. 1995). Another mechanism $^{Y}U^{6+} + {}^{Z}Fe^{2+} = {}^{Y}U^{5+} + {}^{Z}Fe^{3+}$ was proposed for elbrusite (Galuskina et al. 2010a). In our case, the mechanism of Kühberger et al. (1989) leads to major inconsistencies with SIMS data relevant to the hydrogen quantification. Accordingly, the mechanism proposed by Locock et al. (1995) was adopted.

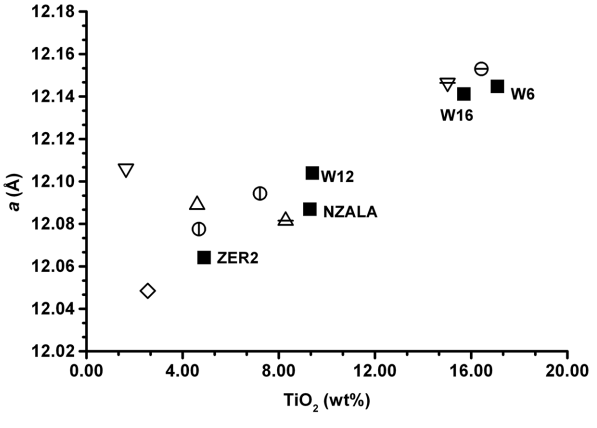

FIGURE 6. Plot of *a* cell parameter vs. TiO_2 (wt%) in Ti-garnets. Symbols as in Figure 1. In addition, circle with vertical line indicates the Magnet Cove andradite from Antao (2013).

For sample NZALA, which contains negligible $^{Z}Fe^{2+}$, our distribution and the one from Grew et al. (2013) are almost identical. Notice that the calculated and measured $Fe^{3+}/\Sigma Fe$ values are very similar (see Tables 2 and 3). Although a general good agreement with X-ray data is observed for both formulas, the difference between $Y\text{-}O_{EPMA}$ and $Y\text{-}O_{X\text{-}ref}$ distances gives <0.01 Å in our case and ~0.02 Å considering only chemical data (see Table 8).

For sample W16, Mössbauer and charge balance derived $Fe^{3+}/\Sigma Fe$ coincide, whereas a discrepancy is observed with respect to the value determined via the Flank method (see Tables 2 and 3 and Fig. 3). The difference between cell parameter from single crystal and powder is $\Delta a \approx 0.01$–0.02 Å. The above evidences indicate that the single crystal is not representative of the powder. Several cation distributions have been checked, until the best fit to the data from different techniques was obtained by considering $Fe^{3+}/\Sigma Fe$ from Flank method and the iron site population from Mössbauer.

Sample W6 has ferrous iron only at tetrahedral site. As in previous sample, inspection of Table 4 evidences that the single crystal has cell parameter shorter than those found in the powder

TABLE 6.—*EXTENDED*

	Ti-rich andradite			Schorlomite	Andradite	Morimotoite		Grossular	Kimzeyite	Melanite
	Antao (2013) Phase I	Antao (2013) Phase II	Antao (2013) Phase III	Chakhmouradian and McCammon (2005)	Adamo et al. (2011)	Antao (2014) Phase I	Antao (2014) Phase II	Novak and Gibbs (1971)	Schingaro et al. (2001)	Scordari et al. (1999)
X1-O	2.3609(8)	2.373(1)	2.3575(8)	2.368(1)	2.3609(7)	2.3631(9)	2.338(3)	2.325(1)	2.409(2)	2.347(1)
X2-O	2.5085(9)	2.505(1)	2.5070(8)	2.515(1)	2.5009(6)	2.5134(9)	2.515(3)	2.482(1)	2.546(2)	2.498(1)
<X-O>	2.4347(9)	2.439(1)	2.4323(8)	2.442(1)	2.4309(7)	2.4383(9)	2.427(3)	2.404(1)	2.478(2)	2.423(1)
Y-O	2.0043(9)	2.003(1)	2.0095(9)	2.006(1)	2.0199(6)	2.011(1)	1.988(3)	1.924(1)	2.050(2)	1.989(1)
Z-O	1.6639(9)	1.671(1)	1.6559(9)	1.689(1)	1.6474(6)	1.693(1)	1.704(3)	1.645(1)	1.738(2)	1.651(1)
<D-O> (Å)	2.134	2.138	2.132	2.145	2.132	2.145	2.136	2.094	2.186	2.121
V_X (Å^3)	24.697	24.773	24.623	24.933	24.528	24.856	25.165	23.800	26.012	24.316
Δ(X-O)	0.148	0.133	0.149	0.148	0.140	0.15	0.127	0.1557	0.136	0.152
α (°)	26.594	26.710	26.745	26.584	27.213	26.803	26.168	24.871	27.368	26.331
V_Y (Å^3)	10.733	10.718	10.815	10.766	10.983	10.847	10.478	9.528	11.507	10.473
OAV (°^{2})	0.670	0.727	0.800	0.062	0.981	0.005	0.297	2.335	0.424	0.94
S(Y) (Å)	2.854	2.853	2.863	2.843	2.880	2.843	2.825	2.754	2.885	2.834
U(Y) (Å)	2.815	2.813	2.820	2.831	2.833	2.846	2.799	2.695	2.917	2.789
t_{SY} (Å)	2.283	2.280	2.285	2.307	2.293	2.325	2.275	2.175	2.394	2.258
t_{UY} (Å)	2.346	2.346	2.355	2.326	2.371	2.320	2.317	2.273	2.343	2.333
X-Y (Å)	3.376	3.380	3.372	3.395	3.371	3.398	3.399	3.314	3.464	3.354
φ(°)	133.72	133.66	133.64	133.30	133.34	132.87	133.89	135.51	132.00	134.04
V_Z (Å^3)	2.336	2.370	2.301	2.441	2.268	2.455	2.516	2.289	2.656	2.286
TAV (°^{2})	32.648	27.230	33.657	36.048	31.309	40.124	24.615	27.066	39.742	32.610
S(Z) (Å)	2.589	2.612	2.575	2.622	2.566	2.621	2.669	2.582	2.691	2.571
U(Z) (Å)	2.779	2.785	2.766	2.824	2.750	2.835	2.837	2.753	2.909	2.759
t_{SZ} (Å)	2.090	2.085	2.083	2.130	2.066	2.145	2.118	2.060	2.201	2.075
t_{UZ} (Å)	1.831	1.847	1.821	1.854	1.815	1.853	1.887	1.826	1.903	1.818
X-Z (Å)	3.019	3.024	3.016	3.037	3.015	3.039	3.040	2.964	3.099	3.000

($\Delta a \approx 0.01$–0.02 Å). Accordingly, for the study single crystal a lower degree of tetrahedral substitution is expected with respect to the analysed powder. The best fit to all the experimental data is obtained varying the $^{Z}Fe^{2+}$ component within one standard deviation.

The main substitution mechanisms affecting the studied garnets are:

(1) $^{Y}R^{4+} + {}^{Z}R^{3+} \leftrightarrow {}^{Z}Si + {}^{Y}R^{3+}$ (schorlomite substitution);
(2) $^{Y}R^{2+} + {}^{Z}R^{4+} \leftrightarrow 2{}^{Y}R^{3+}$ (morimotoite substitution);
(3) $^{Y}R^{3+} \leftrightarrow {}^{Y}Fe^{3+}$ (andradite substitution);

where $^{Y}R^{2+} = Fe^{2+}$, Mg^{2+}, Mn^{2+}; $^{Z}R^{4+} = Ti$; $^{Y}R^{3+} = Fe^{3+}$, Al^{3+}, Cr^{3+}; $^{Z}R^{3+} = Fe^{3+}$, Al^{3+}.

Minor substitutions, such as:

(a) $2{}^{Y}Ti^{4+} + {}^{Z}Fe^{2+} \leftrightarrow 2{}^{Y}Fe^{3+} + {}^{Z}Si$;
(b) $(SiO_4)^{4-} \leftrightarrow (O_4H_4)^{4-}$;
(c) $F^- \leftrightarrow OH^-$;
(d) $^{Y}R^{4+} + {}^{X}R^{+} \leftrightarrow {}^{Y}R^{3+} + {}^{X}Ca^{2+}$,

with $^{Y}R^{4+} = Ti$, Zr; $^{Y}R^{3+} = Fe^{3+}$, Al, Cr^{3+}; $^{X}R^{+} = Na$, Li also occur. On the whole, light elements, although occurring in detectable amounts, do not play a significant crystal chemical role. No systematic trend was here evidenced from the analysis of Ti and water content in relation to the garnets host rocks (see also Fig. 1).

For a better crystal-chemical comparison, in Table 7, in addition to the structural formulas derived for the samples under study, also formulas taken from the literature are reported, selected to include natural end-member garnets (grossular, Novak and Gibbs 1971; andradite, Adamo et al. 2011) as well as Z-substituted Ti garnets for which cation partition was provided on the basis of evidences from multiple methods-combination of chemical and/or X-ray diffraction and/or spectroscopic data (Müntener and Hermann 1994; Ulrych et al. 1994; Locock et al. 1995; Scordari et al. 1999; Schingaro et al. 2001; Chakhmouradian and McCammon 2005; Katerinopoulou et al. 2009; Antao 2013, 2014). It can be seen that the chemical complexity of Ti-garnets is such that every sample has to be considered on a one to one basis. In some cases, to get the best agreement, with X-ray data, Ti has to be distributed over octahedral and tetrahedral site (sample W6 and W16, this work; Scordari et al. 1999; Katerinopoulou et al. 2009). Evidence of the occurrence of Ti at Z site have been reported by Malitesta et al. (1995) and Armbruster at al. (1998) for garnets with similar composition, as well as in Si-poor natural garnets, like elbrusite and bitikleite (Galuskina et al. 2010a, 2010b). The Ti valence state is a controversial topic in the Ti-garnets literature and has been thoroughly reviewed by Grew et al. (2013). In particular, in natural Ti-garnets, Malitesta et al. (1995) found significant Ti^{3+} using X-ray photoelectron spectroscopy (XPS), whereas Waychunas (1987) and Locock et al. (1995) detected low or negligible Ti^{3+} via X-ray absorption near edge structure (XANES) spectroscopy. This discrepancy may be due to a greater contribution of the mineral surface in the case of XPS (Grew et al. 2013) as well as to the problems in the interpretation of XPS signals related to the adopted method of background removing (Guascito et al. 2014). In the present work, the Ti speciation has not been determined by direct measurements, but it was constrained indirectly through the quantification of the water content, the determination of the iron oxidation state and the balance of the substitution mechanisms in garnets.

The two approaches discussed above and used to calculate the crystal-chemical formulas lead to a different classification of the study samples as shown in the plot of Figure 10. In particular, when the only chemical data are used, the samples fall in the schorlomite field together with the Afrikanda schorlomite (Chakhmouradian and McCammon 2005) and the morimotoite (Antao 2014). On the contrary, when the multimethodic approach is used, the study garnets plot in the andradite field very close to most of the considered literature garnets (Müntener and Hermann

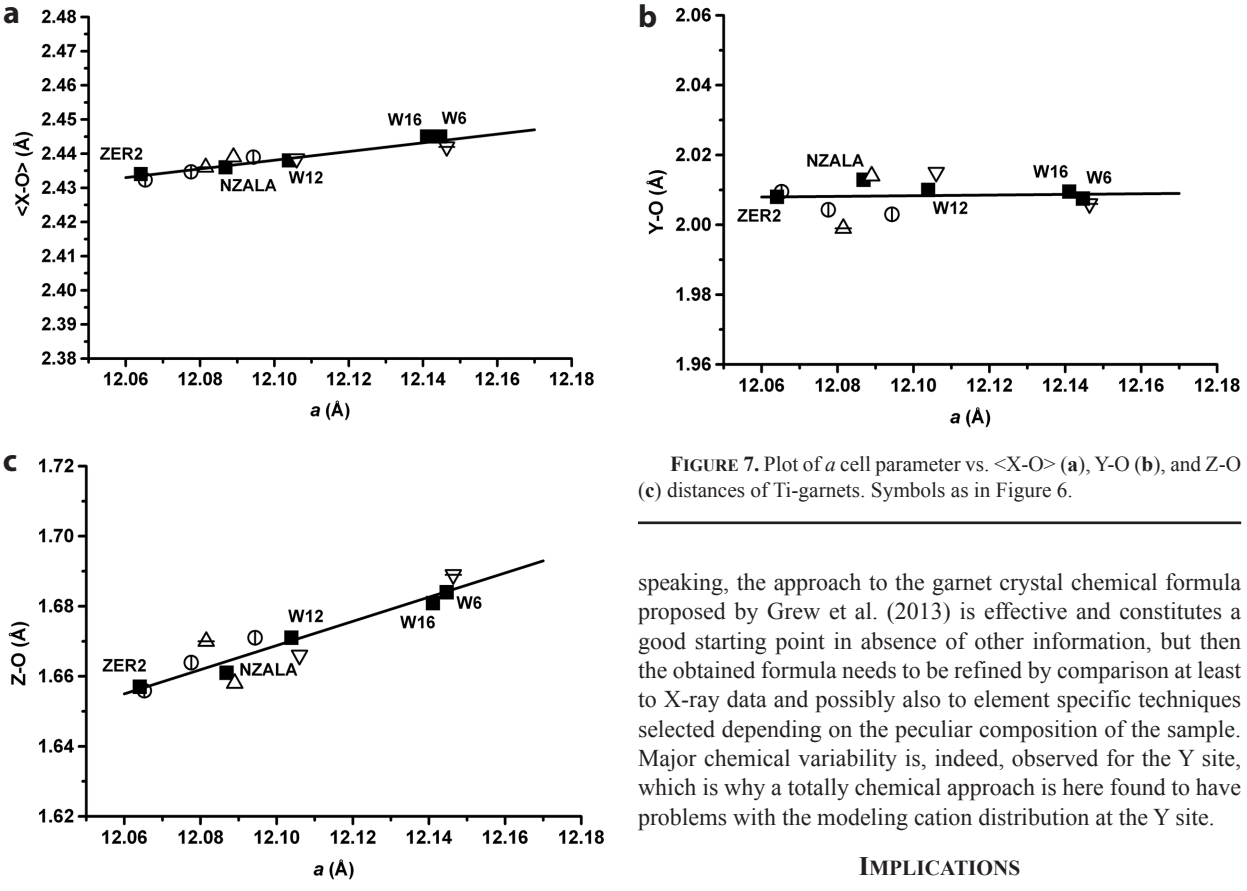

FIGURE 7. Plot of *a* cell parameter vs. <X-O> (**a**), Y-O (**b**), and Z-O (**c**) distances of Ti-garnets. Symbols as in Figure 6.

1994; Ulrych et al. 1994; Locock et al. 1995; Amthauer and Rossman 1998; Katerinopoulou et al. 2009; Phichaikamjornwut et al. 2011; Antao 2013). Notice that kimzeyite sample investigated by Schingaro et al. (2001) should be classified as belonging to the garnet group rather than to schorlomite group. Generally speaking, the approach to the garnet crystal chemical formula proposed by Grew et al. (2013) is effective and constitutes a good starting point in absence of other information, but then the obtained formula needs to be refined by comparison at least to X-ray data and possibly also to element specific techniques selected depending on the peculiar composition of the sample. Major chemical variability is, indeed, observed for the Y site, which is why a totally chemical approach is here found to have problems with the modeling cation distribution at the Y site.

IMPLICATIONS

Garnet is a widespread mineral stable in wide range of temperature (from <300 to 2000 °C) and pressure (from ambient pressure to 25 GPa). The renewed interest in the garnet species is testified by a recent issue of *Elements* [vol. 9(6), December 2013] devoted to the garnet supergroup of minerals. The rel-

TABLE 7. Structural formulas in atoms per formula unit (apfu) of the studied samples, selected literature Ti-garnets and natural end-member garnets

	X site	Y site	Z site
	Cation distribution from this study		
W6	$(Ca_{2.88}Mg_{0.07}Na_{0.05})_{\Sigma=3.00}$	$(Mg_{0.08}Mn_{0.02}Fe^{3+}_{0.88}Ti^{3+}_{0.17}Ti^{4+}_{0.84}Zr_{0.01})_{\Sigma=2.00}$	$(Si_{2.29}Ti_{0.08}Fe^{3+}_{0.38}Fe^{2+}_{0.11}Al_{0.10}\square_{0.04})_{\Sigma=3.00}$
W12	$(Ca_{2.98}Mn_{0.01}Na_{0.01})_{\Sigma=3.00}$	$(Mg_{0.13}Fe^{3+}_{1.18}Al_{0.09}Ti^{3+}_{0.06}Ti^{4+}_{0.54})_{\Sigma=2.00}$	$(Si_{2.58}Fe^{3+}_{0.28}Al_{0.12}\square_{0.02})_{\Sigma=3.00}$
W16	$(Ca_{2.88}Mg_{0.06}Na_{0.06})_{\Sigma=3.00}$	$(Mg_{0.06}Mn_{0.02}Fe^{2+}_{0.15}Fe^{3+}_{0.73}Al_{0.10}Ti^{3+}_{0.11}Ti^{4+}_{0.81}Zr_{0.02})_{\Sigma=2.00}$	$(Si_{2.38}Ti_{0.08}Fe^{3+}_{0.50}Fe^{2+}_{0.02}\square_{0.02})_{\Sigma=3.00}$
NZALA	$(Ca_{2.96}Mg_{0.02}Na_{0.02})_{\Sigma=3.00}$	$(Mg_{0.07}Mn_{0.04}Fe^{2+}_{0.12}Fe^{3+}_{1.09}Cr_{0.01}Al_{0.05}Ti^{4+}_{0.61}Zr_{0.01})_{\Sigma=2.00}$	$(Si_{2.64}Fe^{3+}_{0.29}Al_{0.06}Fe^{2+}_{0.01})_{\Sigma=3.00}$
ZER2	$(Ca_{2.97}Mg_{0.03}Li_{0.01})_{\Sigma=3.01}$	$(Mg_{0.02}Mn_{0.01}Fe^{3+}_{1.46}Cr_{0.01}Al_{0.18}Ti^{3+}_{0.21}Ti^{4+}_{0.10}Zr_{0.01})_{\Sigma=2.00}$	$(Si_{2.88}Al_{0.07}\square_{0.05})_{\Sigma=3.00}$
	Cation distribution after Grew et al. (2013)		
W6	$(Ca_{2.88}Fe_{0.05}Mn_{0.02}Na_{0.05})_{\Sigma=3.00}$	$(Mg_{0.15}Fe^{2+}_{0.23}Fe^{3+}_{0.52}Ti_{1.09}Zr_{0.01})_{\Sigma=2.00}$	$(Si_{2.29}Fe^{3+}_{0.57}Al_{0.10})_{\Sigma=2.96}$
W12	$(Ca_{2.98}Mn_{0.02}Na_{0.01})_{\Sigma=3.01}$	$(Mg_{0.13}Fe^{2+}_{0.06}Fe^{3+}_{1.20}Ti_{0.60})_{\Sigma=1.99}$	$(Si_{2.58}Fe^{3+}_{0.18}Al_{0.21})_{\Sigma=2.97}$
W16	$(Ca_{2.87}Fe_{0.05}Mn_{0.02}Na_{0.06})_{\Sigma=3.00}$	$(Mg_{0.12}Fe^{2+}_{0.24}Fe^{3+}_{0.62}Ti_{1.00}Zr_{0.02})_{\Sigma=2.00}$	$(Si_{2.37}Fe^{3+}_{0.49}Al_{0.10})_{\Sigma=2.96}$
NZALA	$(Ca_{2.96}Mn_{0.02}Na_{0.02})_{\Sigma=3.00}$	$(Mg_{0.10}Mn_{0.02}Fe^{2+}_{0.12}Fe^{3+}_{1.15}Cr_{0.01}Ti_{0.61}Zr_{0.01})_{\Sigma=2.02}$	$(Si_{2.63}Fe^{3+}_{0.24}Al_{0.12})_{\Sigma=2.99}$
ZER2	$(Ca_{2.96}Fe_{0.02}Mn_{0.02})_{\Sigma=3.00}$	$(Mg_{0.06}Fe^{2+}_{0.19}Fe^{3+}_{1.25}Al_{0.19}Cr_{0.01}Ti_{0.31}Zr_{0.01})_{\Sigma=2.02}$	$(Si_{2.87}Al_{0.06}Li_{0.01})_{\Sigma=2.94}$
Müntener and Hermann (1994)	$Ca_{3.00}$	$(Fe^{3+}_{1.24}Fe^{2+}_{0.12}Mn_{0.01}Ca_{0.07}Cr_{0.02}Al_{0.06}Ti^{4+}_{0.31}Ti^{3+}_{0.17})_{\Sigma=2.00}$	$(Si_{2.80}Al_{0.11}\square_{0.09})_{\Sigma=3.00}$
Ulrych et al. (1994)	$(Ca_{2.904}Mg_{0.015}Mn_{0.003}Fe^{2+}_{0.024}Na_{0.011}K_{0.005})_{\Sigma=2.962}$	$(Fe^{3+}_{1.206}Mg_{0.082}Zr_{0.006}Al_{0.551}Ti_{0.155})_{\Sigma=2.000}$	$(Si_{2.799}\square_{0.205})_{\Sigma=3.00}$
Katerinopoulou et al. (2009)	$(Ca_{2.99}Mg_{0.03})_{\Sigma=3.02}$	$(Fe^{3+}_{0.67}Cr_{0.54}Al_{0.33}Ti_{0.29}Zr_{0.15})_{\Sigma=1.98}$	$(Si_{2.42}Al_{0.14}Ti_{0.24}Fe^{3+}_{0.18})_{\Sigma=2.98}$
Antao (2013)	$(Ca_{2.964}Mg_{0.010}Mn_{0.026})_{\Sigma=3.000}$	$(Mg_{0.083}Fe^{3+}_{1.608}Fe^{2+}_{0.006}Cr_{0.001}Al_{0.007}Ti^{4+}_{0.295})_{\Sigma=2.00}$	$(Si_{2.795}Al_{0.205})_{\Sigma=3.000}$
	$(Ca_{2.960}Mg_{0.012}Mn_{0.028})_{\Sigma=3.000}$	$(Mg_{0.121}Fe^{3+}_{1.401}Fe^{2+}_{0.023}Ti^{4+}_{0.455})_{\Sigma=2.00}$	$(Si_{2.689}Al_{0.200}Fe^{3+}_{0.111})_{\Sigma=3.000}$
Adamo et al. (2011)	$Ca_{3.000}$	$(Ti_{0.002}Al_{0.005}Cr_{0.017}Fe^{3+}_{1.952}Mn_{0.001}Mg_{0.016})_{\Sigma=1.993}$	$Si_{3.008}$
Locock et al. (1995)	$(Ca_{2.866}Mn_{0.019}Mg_{0.080}Na_{0.038})_{\Sigma=3.003}$	$(Mg_{0.055}Mn_{0.013}Fe^{2+}_{0.057}Fe^{3+}_{0.631}V^{3+}_{0.014}Al_{0.137}Ti^{4+}_{1.058}Zr_{0.039})_{\Sigma=2.004}$	$(Si_{2.348}Fe^{3+}_{0.339}Fe^{2+}_{0.311}\square_{0.005})_{\Sigma=3.003}$
Chakhmouradian and McCammon (2005)	$(Ca_{2.899}Mn_{0.020}Fe^{2+}_{0.058}Na_{0.023})_{\Sigma=3.000}$	$(Mg_{0.156}Fe^{2+}_{0.197}Fe^{3+}_{0.556}Al_{0.049}Ti_{0.959}Zr_{0.080}Nb_{0.003})_{\Sigma=2.000}$	$(Si_{2.302}Al_{0.171}Fe^{3+}_{0.497}\square_{0.030})_{\Sigma=3.000}$
Antao (2014)	$(Ca_{2.91}Mg_{0.05}Mn^{2+}_{0.03})_{\Sigma=2.99}$	$(Ti_{1.09}Fe^{3+}_{0.46}Fe^{2+}_{0.37}Mg_{0.08})_{\Sigma=2.00}$	$(Si_{2.36}Al_{0.14}Fe^{3+}_{0.51})_{\Sigma=3.01}$
Novak and Gibbs (1971)	$(Ca_{2.96}Mn_{0.04})_{\Sigma=3.00}$	$(Al_{1.95}Fe_{0.05})_{\Sigma=2.00}$	$Si_{3.00}$
Schingaro et al. (2001)	$(Ca_{2.97}Ba^{2+}_{0.03})_{\Sigma=3.00}$	$(Mg_{0.11}REE^{3+}_{0.02}Zr^{4+}_{1.12}Ti^{4+}_{0.68}Fe^{3+}_{0.07})_{\Sigma=2.00}$	$(Si_{1.33}Al_{0.81}Fe^{3+}_{0.85})_{\Sigma=2.99}$
Scordari et al. (1999)	$(Ca_{2.75}Mg_{0.05}Mn^{2+}_{0.07}Fe^{2+}_{0.13})_{\Sigma=3.00}$	$(Ti^{4+}_{0.04}Ti^{3+}_{0.12}Fe^{3+}_{1.12}Fe^{2+}_{0.05}Al_{0.67})_{\Sigma=2.00}$	$(Si_{2.88}Ti_{0.05}Fe^{3+}_{0.04})_{\Sigma=2.97}$

(Table extends to next page)

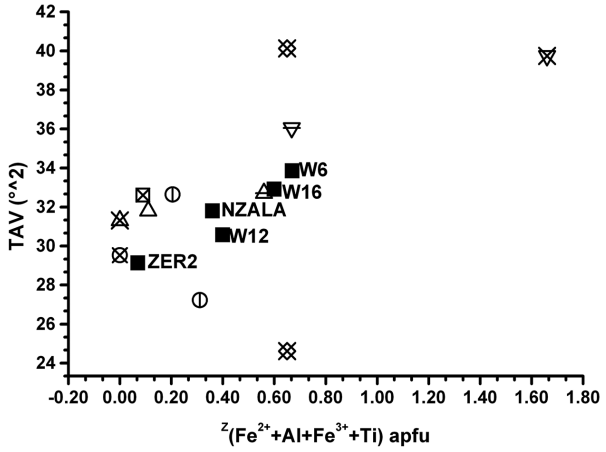

FIGURE 8. Plot of tetrahedral angle variance (TAV parameter) vs. (Fe^{2+}+Al+Fe^{3+}+Ti) amount in the tetrahedral site of Ti-garnets and natural end-member garnets. Symbols as in Figure 6. Other symbols: circle with cross inside = Novak and Gibbs (1971); square with cross inside = Scordari et al. (1999); pointing downward triangle with cross inside = Schingaro et al. 2001; pointing upward triangle with cross inside = Adamo et al. (2011); diamond with cross inside = Antao (2014).

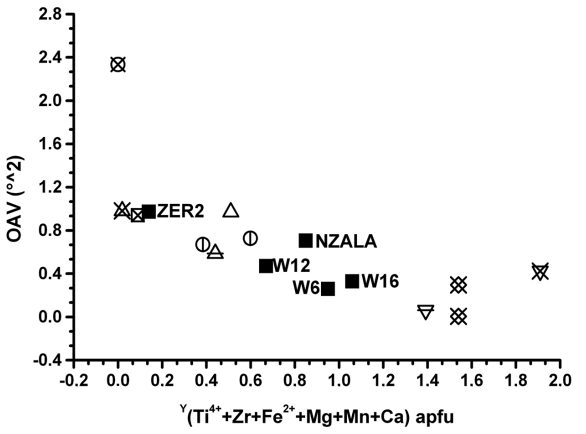

FIGURE 9. Plot of octahedral angle variance (OAV parameter) vs. (Ti^{4+}+Zr+Fe^{2+}+Mg+Mn+Ca) amount in the octahedral site of Ti-garnets and natural end-member garnets. Symbols as in Figure 8.

evance of elemental substitutions in determining the properties of garnets has been highlighted in Grew et al. (2013), Geiger (2013), and Antao (2013). In particular, Grew et al. (2013) evidence that recently (2009–2010) 10 new garnet species with unusual constituents were approved by the Commission on New Minerals, Nomenclature and Classification of the International Mineralogical Association and the 32 approved species also encompass three ungrouped species but new species are expected due to the extreme compositional variations in natural garnets. Geiger (2013), other than reviewing synthetic non-silicate garnets and the relevant technological employment, stresses the significance of studying substitutional solid solutions in natural garnets. Cation substitutions involve strain fields resulting in structural heterogeneities from the scale of the unit cell to the nanoscale. Structural and chemical bonding properties of garnets are believed to control element partitioning (Wood et al. 2013) and thermodynamic behavior of the garnet solid solutions. For a complete characterization of these phases, both techniques sensitive to long-range ordering (such as X-ray diffraction) and to short range ordering (spectroscopic techniques) are needed. This is the approach adopted in the present work. Regarding natural Ti-garnets, their relevance from a petrological point of view has been mentioned in the introduction section. However, it is generally recognized that determination of cation site population is really complicated for such compositions. In turn, cation exchange mechanisms produce polyhedral distortions, which have been reported here, but unravelling the contribution of each of the multiple substitutions requires further work. In this study, the detailed characterization of substitution mechanisms by single-crystal X-ray diffraction is associated to the observation

TABLE 7.—*EXTENDED*

	φ site	SIMS data
Cation distribution from this study:		
W6	$O_{11.84}OH_{0.16}$	$OH_{0.17}F_{0.002}Li_{0.001}$
W12	$O_{11.92}OH_{0.08}$	$OH_{0.10}F_{0.003}Li_{0.001}$
W16	$O_{11.92}OH_{0.07}F_{0.01}$	$OH_{0.12}F_{0.010}Li_{0.001}$
NZALA	$O_{12.00}$	$OH_{0.05}F_{0.005}Li_{0.003}$
ZER2	$O_{11.80}OH_{0.20}$	$OH_{0.25}F_{0.001}Li_{0.005}$
Cation distribution after Grew et al. (2013):		
W6	$O_{11.82}OH_{0.18}$	
W12	$O_{11.90}OH_{0.10}$	
W16	$O_{11.86}OH_{0.13}F_{0.01}$	
NZALA	$O_{11.94}OH_{0.05}F_{0.01}$	
ZER2	$O_{11.74}OH_{0.26}$	
Müntener and Hermann (1994)	$O_{11.64}OH_{0.36}$	
Ulrych et al. (1994)	$O_{11.181}OH_{0.792}F_{0.028}$ $Na_{0.011}K_{0.005})_{\Sigma=2.962}$	
Katerinopoulou et al. (2009)	$O_{11.89}OH_{0.1}$	
Antao (2013)	$O_{12.000}$ $O_{12.000}$	
Adamo et al. (2011)	O_{12}	
Locock et al. (1995)	O_{12}	
Chakhmouradian and McCammon (2005)	$O_{11.880}OH_{0.120}$	
Antao (2014)	O_{12}	
Novak and Gibbs (1971)	O_{12}	
Schingaro et al. (2001)	O_{12}	
Scordari et al. (1999)	$O_{11.83}OH_{0.17}$	

TABLE 8. Comparison of refined bond distances (Å) and mean atomic numbers (electrons, e^-) of cation sites as determined by structure refinement (X-ref) and EPMA for the studied crystals

	W6	W12	W16	NZALA	ZER2
Y-$O_{X\text{-ref}}$	2.008(1)	2.008(1)	2.010(1)	2.0121(4)	2.009(1)
Y-O_{EPMA}[a]	2.014	2.015	2.018	2.022	2.017
Y-O_{EPMA}[b]	2.025	2.019	2.026	2.032	2.030
Z-$O_{X\text{-ref}}$	1.684(1)	1.671(1)	1.681(1)	1.6615(4)	1.656(1)
Z-O_{EPMA}[a]	1.696	1.669	1.687	1.666	1.648
Z-O_{EPMA}[b]	1.692	1.666	1.689	1.665	1.650
m.a.n.$(X)_{X\text{-ref}}$	20.00	20.00	20.00	20.00	20.00
m.a.n.$(X)_{EPMA}$[a]	19.66	19.99	19.66	19.89	19.93
m.a.n.$(X)_{EPMA}$[b]	19.98	20.07	19.95	19.97	20.07
m.a.n.$(Y)_{X\text{-ref}}$	22.50	22.52	22.46	23.31	23.30
m.a.n.$(Y)_{EPMA}$[a]	23.48	23.31	23.22	24.01	24.13
m.a.n.$(Y)_{EPMA}$[b]	22.84	23.76	23.30	24.39	24.05
m.a.n.$(Z)_{X\text{-ref}}$	15.85	14.75	15.74	14.61	14.00
m.a.n.$(Z)_{EPMA}$[a]	15.95	14.99	16.20	15.18	13.74
m.a.n.$(Z)_{EPMA}$[b]	16.06	14.51	15.74	14.87	13.66

Note: Average error on mean atomic number ±0.5 e^-.
[a] According to our cation distribution.
[b] According to the Grew et al. (2013) cation distribution.

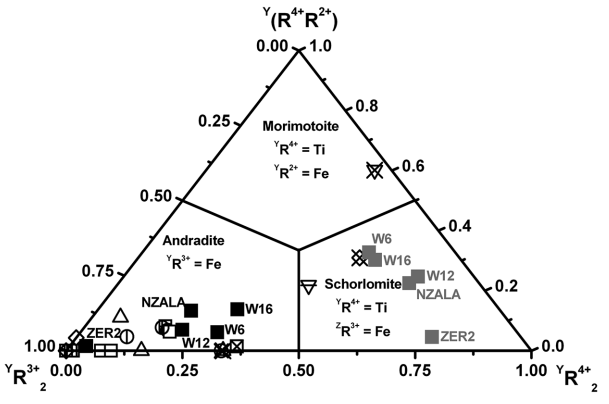

Figure 10. Classification diagram for the studied and selected literature hydrogarnets. Symbols as in Figure 8. Gray symbols indicate the studied samples whose formulas have been calculated according to Grew et al. (2013). In addition, square with horizontal line represents GA34, GRR134, GRR169, GRR684, GRR1328, GRR1765, GA32, GA35, GRR149, GRR1015, GRR1447, GA24, GA36, GRR1446, and CITH3110 samples from Amthauer and Rossman (1998).

of occurrence of multiple cubic phases from laboratory XRPD data. Even if, in our case, the samples appeared homogeneous at the EPMA scale it is here suggested that compositional differences at the nanoscale may occur, as found by other authors (Antao 2013). These findings, in turn, may have implication for the study of garnets zonation (see, for instance, Matthews et al. 1992; Gwalani et al. 2000; Agrosì et al. 2002, 2011). Complex zoning occurring in primary Ti-garnets and involving variation of Ca, Ti, Zr, and Al was described by Gwalani et al. (2000). These authors were able to correlate it to the multiple events that occurred during the magma crystallization, depicting a multistep magmatic history from fractional crystallization, to magma mixing to crystallization in closed system, to fluctuation of *P-T*, f_{O_2} conditions. Agrosì et al. (2002) studied the sector zoning in Ti-andradite from Colli Albani and found that morimotoite substitution was present in {110} sectors, whereas both morimotoite and schorlomite substitutions affected {121} sectors. The strain associated to the presence of the schorlomite substitution in {121} sectors could be correlated to the higher growth rate of these sectors with respect to the others by the layer-by layer mechanism. Subsequently, for the same Ti-garnets from Colli Albani concentric zoning was also observed, that, together with the identification of growth marks, allowed to characterize the growth environment (Agrosì et al. 2011). Very recently (Antao et al. 2015) correlated the occurrence of multiple cubic phases in Ti-rich andradite to optical anomalies (birefringence) and to oscillatory zoning related to andradite-rich and andradite-poor cubic phases or to subtle chemical variations involving Ti, Fe, Al, and Mg atoms concentrations. All the above considerations indicate the high sensitivity of the Ti-garnet structure in that even slight element abundance variation has detectable effect on the crystal structure (in terms of cell edges, bond distances, etc.) as well as the potential use of the garnet crystal chemistry at the micrometric or even nanometric scale to derive geological inferences (i.e. magma evolution, thermal history, growth environment, late-stage reactions, etc.).

Acknowledgments

The authors are grateful to Stefano Poli (University of Milano) for the facilities at the Electron Microprobe Laboratory and Nadia Malaspina for the assistance during the "Flank method" analyses at the Dipartimento di Scienze della Terra, University of Milano. Thomas Armbruster is gratefully thanked for providing NZALA and ZER2 garnet samples. Thanks are due to the Associate Editor, Gatta Giacomo Diego, and to Redhammer Günther Josef and a anonymous Referee that contributed to significantly improve the manuscript.

The XRPD laboratory at the Dipartimento di Scienze della Terra and Geoambientali, University of Bari "Aldo Moro," was funded by Potenziamento Strutturale PONa3_00369 "Laboratorio per lo Sviluppo Integrato delle Scienze e delle TEcnologie dei Materiali Avanzati e per dispositivi innovativi (SISTEMA)."

This work was also supported by the COFIN-MIUR.

References cited

Adamo, I., Gatta, G.D., Rotiroti, N., Diella, V., and Pavese, A. (2011) Green andradite stones: gemmological and mineralogical characterisation. European Journal of Mineralogy, 23, 91–100.

Agrosì, G., Schingaro, E., Pedrazzi, G., Scandale, E., and Scordari, F. (2002) A crystal chemical insight into sector zoning of a titanian andradite ("melanite") crystal. European Journal of Mineralogy, 14(1), 785–794.

Agrosì, G., Scandale, E., and Tempesta, G. (2011) Growth marks of titanian-andradite crystals from Colli Albani (Italy). Periodico di Mineralogia, 80(1), 89–104.

Amthauer, G., and Rossman, G.R. (1998) The hydrous component in andradite garnet. American Mineralogist, 83, 835–840.

Antao, S.M. (2013) The mystery of birefringent garnet: is the symmetry lower than cubic? Powder Diffraction, 28(4), 281–288.

——— (2014) Crystal structure of morimotoite from Ice River, Canada. Powder diffraction, 29(4), 325–330.

Antao, S.M., and Klincker, A.M. (2013) Origin of birefringence in andradite from Arizona, Madagascar, and Iran. Physics and Chemistry of Minerals, 40, 575–586.

Antao, S.M., and Round, S.A. (2014) Crystal chemistry of birefringent spessartine. Powder Diffraction, 29(3), 233–240.

Antao, S.M., Mohib, S., Zaman, M., and Marr, R.A. (2015) Ti-rich andradites: chemistry, structure, multi-phases, optical anisotropy, and oscillatory zoning. Canadian Mineralogist, DOI: 10.3749/canmin.1400042.

Armbruster, T. (1995) Structure refinement of hydrous andradite, $Ca_3Fe_{1.54}Mn_{0.20}Al_{0.26}(SiO_4)_{1.65}(O_4H_4)_{1.35}$, from the Wessels mine, Kalahari manganese field, South Africa. European Journal of Mineralogy, 7, 1221–1225.

Armbruster, T., Birrer, J., Libowitzky, E., and Beran, A. (1998) Crystal chemistry of Ti-bearing andradites. European Journal of Mineralogy, 10, 907–921.

Balić-Žunić, T., and Vicković, I. (1996) IVTON—a program for the calculation of geometrical aspects of crystal structures and some crystal chemical applications. Journal of Applied Crystallography, 29, 305–306.

Barbanson, L., and Bastos Neto, A.C. (1992) Hydroandradite titanifère fluorée et grenat ($Spe_{39}Gro_{31}Alm_{23}And_6$) fluoré des granitoïdes du district à fluorine de Santa Catarina (Brésil): description minéralogique, mécanisme d'incorporation du fluor, signification pétrologique et métallogénique. Comptes Rendus de l'Académie des Sciences, Série II, 314, 63–69.

Basso, R., and Cabella, R. (1990) Crystal chemical study of garnets from metarodingites in the Voltri Group metaophiolites (Ligurian Alps, Italy). Neues Jahrbuch für Mineralogie Monatshefte, 127–136.

Basso, R., Cimmino, F., and Messiga, B. (1984a) Crystal chemistry of hydrogarnets from three different microstructural sites of a basaltic metarodingite from the Voltri Massif (Western Liguria, Italy). Neues Jahrbuch für Mineralogie Abhandlungen, 148, 246–258.

Basso, R., Cimmino, F., and Messiga, B. (1984b) Crystal chemical and petrological study of hydrogarnets from a Fe-gabbro metarodingite (Gruppo di Voltri, Western Liguria, Italy). Neues Jahrbuch für Mineralogie Abhandlungen, 150, 247–258.

Bell, D.R., Rossman, G.R., and Moore, R.O. (2004) Abundance and partitioning of OH in a high-pressure magmatic system: megacrysts from the Monastery kimberlite, South Africa. Journal of Petrology, 45(8), 1539–1564.

Betteridge, P.W., Carruthers, J.R., Cooper, R.I., Prout, K., and Watkin, D.J. (2003) Crystals version 12: software for guided crystal structure analysis. Journal of Applied Crystallography, 36, 1487.

Born, L., and Zemann, J. (1964) Abstandsberechnungen und gitterenergetische Berechnungen an Granaten. Contributions to Mineralogy and Petrology, 10, 2–23.

Brod, J.A., Junqueira-Brod, T.C., Gaspar, J.C., Gibson, S.A., and Thompson, R.N. (2003) Ti-rich and Ti-poor garnet from the Tapira carbonatite complex, SE Brazil: fingerprinting fractional crystallization and liquid immiscibility. In 8th International Kimberlite Conference, Extended Abstracts (CD), FLA_0399.pdf, p. 5.

Bruker (2003a) COSMO (ver. 1.61), Bruker AXS Inc., Madison, Wisconsin, USA.

——— (2003b) SAINT (ver. 7.60A). Bruker AXS Inc., Madison, Wisconsin, USA.

Cempírek, J., Novák, M., Dolníček, Z, Kotková, J., and Škoda, R. (2010) Crystal

chemistry and origin of grandidierite, ominelite, boralsilite, and werdingite from the Bory Granulite Massif, Czech Republic. American Mineralogist, 95, 1533–1547.
Chakhmouradian, A.R., and McCammon, C.A. (2005) Schorlomite: a discussion of the crystal chemistry, formula, and inter-species boundaries. Physics and Chemistry of Minerals, 32, 277–289.
Chakhmouradian, A.R., Cooper, M.A., Medici, L., Hawthorne, F.C., and Adar, F. (2008) Fluorine-rich hibschite from silicocarbonatite, Afrikanda complex, Russia: crystal chemistry and conditions of crystallization. Canadian Mineralogist, 46, 1033–1042.
Cussen, E.J. (2006) The structure of lithium garnets: cation disorder and clustering in a new family of fast Li^+ conductors. Chemical Communications, 4, 412–413.
Deer, W.A., Howie, R.A., and Zussman, J. (1982) Rock-forming minerals, Orthosilicates, 1A, Longman, New York.
Dingwell, D.B., and Brearley, M. (1985) Mineral chemistry of igneous melanite garnets from analcite-bearing volcanic rocks, Alberta, Canada. Contributions to Mineralogy and Petrology, 90, 29–35.
Dwarzski, R.E., Draper, D.S., Shearer, C.K., and Agee, C.B. (2006). Experimental insights on crystal chemistry of high-Ti garnets from garnet-melt partitioning of rare-earth and high-field-strength elements. American Mineralogist, 91(1), 1536–1546.
Dyar, M.D., Schaefer, M.W., Sklute, E.C., and Bishop, J.L. (2008) Mössbauer spectroscopy of phyllosilicates: effect of fitting models on recoil-free fractions and redox ratios. Clay Minerals, 43, 3–33.
Dyar, M.D., Breves, E.A., Emerson, E., Bell, S.W., Nelms, M., Ozanne, M.V., Pell, S.E., Carmosino, M.L., Tucker, J.M., Gunter, M.E., and others. (2012) Accurate determination of ferric iron in garnets by bulk Mössbauer spectroscopy and synchrotron micro-XANES. American Mineralogist, 97, 1726–1740.
Eeckhout, S.G., Castañeda, C., Ferreira, A.C.M., Sabioni, A.C.S., de Grave, E., and Vasconcelos, D.C.L. (2002) Spectroscopic studies of spessartine from Brazilian pegmatites. American Mineralogist, 87, 1297–1306.
Faryad, S.W., and Dianiška, I. (2003) Ti-bearing andradite-prehnite-epidote assemblage from the Malá Fatra granodiorite and tonalite (Western Carpathians). Schweizerische Mineralogische und Petrographische Mitteilugen, 83, 47–56.
Ferro, O., Galli, E., Papp, G., Quartieri, S., Szakáll, S., and Vezzalini, G. (2003) A new occurrence of katoite and re-examination of the hydrogrossular group. European Journal of Mineralogy,15, 419–426.
Flohr, M.J.K., and Ross, M. (1989) Alkaline igneous rocks of Magnet Cove, Arkansas: Metasomatized ijolite xenoliths from Diamond Jo quarry. American Mineralogist, 74, 113–131.
Freiberger, R., Hecht, L., Cuney, M., and Morteani, G. (2001) Secondary Ca-Al silicates in plutonic rocks: implications for their cooling history. Contributions to Mineralogy and Petrology, 141, 415–429.
Galuskin, E.V. (2005) Minerals of the vesuvianite group from the achtarandite rocks (Wiluy River, Yakutia), 191 p. University of Silesa Publishing House, Katowice, Poland (in Polish).
Galuskina, I.O., Galuskin, E.V., Armbruster, T., Lazic, B., Kusz, J., Dzierżanowski, P., Gazeev, V.M., Pertsev, N.N., Prusik, K., Zadov, A.E., and others. (2010a) Elbrusite-(Zr)—A new uranian garnet from the Upper Chegem caldera, Kabardino-Balkaria, Northern Caucasus, Russia. American Mineralogist, 95, 1172–1181.
Galuskina, I.O., Galuskin, E.V., Armbruster, T., Lazic, B., Dzierżanowski, P., Gazeev, V.M., Prusik, K., Pertsev, N.N., Winiarski, A., Zadov, A.E., and others. (2010b) Bitikleite-(SnAl) and bitikleite-(ZrFe): New garnets from xenoliths of the Upper Chegem volcanic structure, Kabardino-Balkaria, Northern Caucasus, Russia. American Mineralogist, 95, 959–967.
Geiger, C.A. (2013) Garnet: a key phase in nature, the laboratory and technology. Elements, 9(6), 447–452.
Geller, S. (1971) Refinement of the crystal structure of cryolithionite, $\{Na_3\}[Al_2](Li_3)F_{12}$. American Mineralogist, 56, 18–23.
Grew, E.S., Chernosky, J.V., Werding, G., Abraham, K., Marquez, N., and Hinthorne, J.R. (1990) Chemistry of kornerupine and associated minerals, a wet chemical, ion microprobe, and X-ray study emphasizing Li, Be, B and F contents. Journal of Petrology, 31(5), 1025–1070.
Grew, E.S., Locock, A.J., Mills, S.J., Galuskina, I.O., Galuskin, E.V., and Hålenius, U. (2013) Nomenclature of the Garnet Supergroup. American Mineralogist, 98, 785–811.
Guascito, M.R., Mesto, E., Malitesta, C., Picca, R.A., and Scordari, F. (2014) The effect of XPS background removing method on the appraisal of Ti and Fe: The case of phlogopites and brookite. American Mineralogist, 99, 139–148.
Gwalani, L.G., Rock, N.M.S., Ramasamy, R., Griffin, B.J., and Mulai, B.P. (2000) Complexly zoned Ti-rich melanite-schorlomite garnets from Ambadungar carbonatite-alkalic complex, Deccan Igneous Province, Gujarat State, Western India. Journal of Asian Earth Sciences, 18, 163–176.
Howie, R.A., and Woolley, A.R. (1968) The role of titanium and the effect of TiO_2 on the cell-size, refractive index, and specific gravity in the andradite-melanite-schorlomite series. Mineralogical Magazine, 36, 775–790.
Höfer, H.E., and Brey, G.P. (2007) The iron oxidation state of garnet by electron microprobe: Its determination with the flank method combined with major-element analysis. American Mineralogist, 92, 873–885.
Huggins, F.E., Virgo, D., and Huckenholz, H.G. (1977a) Titanium-containing silicate garnets. I. The distribution of Al, Fe^{3+}, and Ti^{4+} between octahedral and tetrahedral sites. American Mineralogist, 62, 475–490.
——— (1977b) Titanium-containing silicate garnets. II. The crystal chemistry of melanites and schorlomites. American Mineralogist, 62, 646–655.
Kalinichenko, A.M., Proshko, V.Ya., Matiash, I.V., Pavlishin, V.I., and Garmanik, M.Ya. (1987) NMR data on crystallochemical features of hydrogrossular. Geochemistry International, 24(4), 132–135 (translated from Geokhimiya, 9, 1363–1366, 1986).
Katerinopoulou, A., Katerinopoulos, A., Voudouris, P., Bieniok, A., Musso, M., and Amthauer, G. (2009) A multi-analytical study of the crystal structure of unusual Ti-Zr-Cr-rich Andradite from the Maronia skarn, Rhodope massif, western Thrace, Greece. Mineralogy and Petrology, 95, 113–124.
Koga, K., Hauri, E., Hirschmann, M., and Bell, D. (2003) Hydrogen concentration analyses using SIMS and FTIR: Comparison and calibration for nominally anhydrous minerals. Geochemistry Geophysics Geosystems, 4(2), 1–20.
Kühberger, A., Fehr, T., Huckenholz, H.G., and Amthauer, G. (1989) Crystal chemistry of a natural schorlomite and Ti-andradites synthesized at different oxygen fugacities. Physics and Chemistry of Minerals, 16, 734–740.
Lagarec, K., and Rancourt, D.G. (1997) Extended Voigt-based analytic lineshape method for determining *N*-dimensional correlated hyperfine parameter distributions in Mössbauer spectroscopy. Nuclear Instruments and Methods in Physics Research B, 129, 266–280.
——— (1998) RECOIL, Mössbauer Spectral Analysis Software for Windows (version 1.0). Department of Physics, University of Ottawa, Canada.
Lager, G.A., Armbruster, T., and Faber, J. (1987) Neutron and X-ray diffraction study of hydrogarnet $Ca_3Al_2(O_4H_4)_3$. American Mineralogist, 72, 756–765.
Lager, G.A., Armbruster, T., Rotella, F.J., and Rossman, G.R. (1989) OH substitution in garnets: X-ray and neutron diffraction, infrared, and geometric-modeling studies. American Mineralogist, 74, 840–851.
Locock, A., Luth, R.W., Cavell, R.G., Smith, D.G.W., and Duke, M.J.M. (1995) Spectroscopy of the cation distribution in the schorlomite species of garnet. American Mineralogist, 80, 27–38.
Lupini, L., Williams, C.T., and Wooley, A.R. (1992) Zr-rich garnet and Zr- and Th-rich perovskite from the Polino carbonatite, Italy. Mineralogical Magazine, 56, 581–586.
Malaspina, N., Poli, S., and Fumagalli, P. (2009) The oxidation state of metasomatized mantle wedge: insights from C–O–H-bearing garnet peridotite. Journal of Petrology, 50, 1533–1552.
Malaspina, N., Langenhorst, F., Fumagalli, P., Tumiati, S., and Poli, S. (2012) Fe^{3+} distribution between garnet and pyroxenes in mantle wedge carbonate-bearing garnet peridotites (Sulu, China) and implications for their oxidation state. Lithos, 146–147, 11–17.
Maldener, J., Hösch, A., Langer, K., and Rauch, F. (2003) Hydrogen in some natural garnets studied by nuclear reaction analysis and vibrational spectroscopy. Physics and Chemistry of Minerals, 30, 337–344.
Malitesta, C., Losito, I., Scordari, F., and Schingaro, E. (1995) XPS investigation of titanium in melanites from Monte Vulture (Italy). European Journal of Mineralogy, 7, 847–858.
Manning, C.E., and Bird, D.K. (1990) Fluorian garnets from the host rocks of the Skaergaard intrusion: implications for metamorphic fluid composition. American Mineralogist, 75, 859–873.
Matthews, M., Harte, B., and Prior, D. (1992) Mantle garnets: A cracking yarn. Geochimica et Cosmochimica Acta, 56(7), 2633–2642.
Merli, M., Callegari, A., Cannillo, E., Caucia, F., Leona, M., Oberti, R., and Ungaretti, L. (1995) Crystal-chemical complexity in natural garnets: structural constraints on chemical variability. European Journal of Mineralogy, 7, 1239–1249.
Müntener, O., and Hermann, J. (1994) Titanian andradite in a metapyroxenite layer from the Malenco ultramafics (Italy): implications for Ti-mobility and low oxygen fugacity. Contributions to Mineralogy and Petrology, 116, 156–168.
Novak, G.A., and Gibbs, G.V. (1971) The crystal chemistry of the silicate garnets. American Mineralogist, 56, 791–825.
Onuki, H., Akasaka, M., Yoshida, T., and Nedachia, M. (1982) Ti-Rich Hydroandradites from the Sanbagawa Metamorphic Rocks of the Shibukawa Area, Central Japan. Contributions to Mineralogy and Petrology, 80, 183–188.
Ortalli, I., Pedrazzi, G., Schingaro, E., and Scordari, F. (1994) Iron site populations from Mössbauer spectroscopy in Ti-bearing garnets from Mt. Vulture (Italy). Hyperfine Interactions, 91, 727–732.
Ottolini, L., and Hawthorne, F.C. (2001) SIMS ionization of hydrogen in silicates: a case study of kornerupine. Journal of Analytical Spectrometry, 16, 1266–1270.
Ottolini, L., Bottazzi, P., Zanetti, A., and Vannucci, R. (1995) Determination of Hydrogen in Silicates by Secondary Ion Mass Spectrometry. The Analyst, 120, 1309–1313.
Ottolini, L., Camara, F., Hawthorne, F.C., and Stirling, J. (2002) SIMS matrix effects in the analysis of light elements in silicate minerals: Comparison with SREF and EMPA data. American Mineralogist, 87, 1477–1485.
Pedrazzi, G., Schingaro, E., and Scordari, F. (1998) X-ray single crystal and Mössbauer study on Ti-garnets from the Tapira alkaline-carbonatite complex, Brazil. In E.B. Saitovitch, H. Rechenberg, and R.B. Scorzelli, Eds., Hyperfine Interactions (C), 3, 321–324.

——— (2002) Mössbauer investigation on Ti-garnets from different geological environments. In M.F. Thomas, J.M. Williams, and T.C. Gibb, Eds., Hyperfine Interactions (C), 5, 457–460.

Phichaikamjornwut, B., Skogby, H., Ounchanum, P., Limtrakun, P., and Boonsoong, A. (2011) Hydrous components of grossular-andradite garnets from Thailand: thermal stability and exchange kinetics. European Journal of Mineralogy, 24, 107–121.

Platt, R.G., and Mitchell, R.H. (1979) The Marathon Dikes. I: Zirconium-rich titanian garnets and manganoan magnesian ulvöspinel-magnetite spinels. American Mineralogist, 64, 546–550.

Robinson, K., Gibbs, G.V., and Ribbe, P.H. (1971) Quadratic Elongation: A Quantitative Measure of Distortion in Coordination Polyhedra. Science, 172, 567–570.

Rossman, G.R., and Aines, R.D. (1991) The hydrous components in garnets: Grossular-hydrogrossular. American Mineralogist, 76, 1153–1164.

Saha, A., Ray, J., Ganguly, S., and Chatterjee, N. (2011) Occurrence of melanite garnet in syenite and ijolite-melteigite rocks of Samchampi-Samteran alkaline complex, Mikir Hills, Northeastern India. Current Science, 101(1), 95–100.

Schingaro, E., Scordari, F., Capitanio, F., Parodi, G., Smith, D., and Mottana, A. (2001) Crystal chemistry of kimzeyte from Anguillara, Mts. Sabatini, Italy. European Journal of Mineralogy, 13, 749–759.

Schingaro, E., Scordari, F., Pedrazzi, G., and Malitesta, C. (2004) Ti and Fe speciation by X-ray Photoelectron Spectroscopy (XPS) and Mössbauer Spectroscopy for a full crystal chemical characterisation of Ti-garnets from Colli Albani (Italy). Annali di chimica, 94, 185–196.

Scordari, F., Schingaro, E., and Pedrazzi, G. (1999) Crystal chemistry of melanite from Mt. Vulture (Southern Italy). European Journal of Mineralogy, 11, 855–869.

Scordari, F., Dyar, M.D., Schingaro, E., Lacalamita, M., and Ottolini, L. (2010) XRD, micro-XANES, EMPA, and SIMS investigation on phlogopite single crystals from Mt. Vulture (Italy). American Mineralogist, 95, 1657–1670.

Shannon, R.D. (1976) Revised effective ionic radii and systematic studies of interatomic distances in halides and chalcogenides. Acta Crystallogaphica, A32, 751–767.

Sheldrick, G.M. (2003) SADABS, Program for Empirical Absorption Correction of Area Detector Data. University of Göttingen, Germany.

Shenoy, G.K., Wagner, F.E., and Kalvius, G.M. (1978) The measurement of the isomer shift. In G.K. Schenoy and F.E. Wagner, Eds., Mössbauer Isomer Shifts, p. 49–110. North-Holland Publishing, Amsterdam.

Toby, B.H., and Von Dreele, R.B. (2013) GSAS-II: the genesis of a modern open-source all purpose crystallography software package. Journal of Applied Crystallography, 46(2), 544–549.

Ulrych, J., Povondra, P., Pivec, E., Rutšek, J., and Sitek, J. (1994) Compositional evolution of metasomatic garnet in melilitic rocks of the Osečná complex, Bohemia. Canadian Mineralogist, 32, 637–647.

Ungaretti, L., Leona, M., Merli, M., and Oberti, R. (1995) Non-ideal solid-solution in garnet: crystal-structure evidence and modelling. European Journal of Mineralogy, 7, 1299–1312.

Valley, J.W., Essene, E.J., and Peacor, D.R. (1983) Fluorine-bearing garnets in Adirondack calc-silicates. American Mineralogist, 68, 444–448.

Visser, D. (1993) Fluorine-bearing hydrogarnets from Blengsvatn, Bamble sector, south Norway. Mineralogy and Petrology, 47, 209–218.

Wang, Y., and Lai, W. (2012) High ionic conductivity lithium garnet oxides of $Li_{7-x}La_3Zr_{2-x}Ta_xO_{12}$ compositions. Electrochemical and Solid-State Letters, 15(5), A68–A71.

Watkin, D. (2008) Structure refinement: some background theory and practical strategies. Journal of Applied Crystallography, 41, 491–522.

Waychunas, G.A. (1987) Synchrotron radiation XANES spectroscopy of Ti in minerals: Effects of Ti bonding distances, Ti valence, and site geometry on absorption edge structure. American Mineralogist, 72, 89–101.

Wood, B.J., Kiseeva, E.S., and Matzen, A.K. (2013) Garnet in the Earth's mantle. Elements, 9, 421–426.

Yang, H., Konzett, J., Downs, R.T., and Frost, D.J. (2009) Crystal structure and Raman spectrum of a high-pressure Li-rich majoritic garnet, $(Li_2Mg)Si_2(SiO_4)_3$. American Mineralogist, 94, 630–633.

Young, R.A., Ed. (1993) The Rietveld Method, 308 p. International Union of Crystallography, Oxford Science Publications.

Manuscript received May 28, 2015
Manuscript accepted August 12, 2015
Manuscript handled by G. Diego Gatta